Coherent Bremsstrahlung, Coherent Pair Production, Birefringence and Polarimetry in the 20-170 GeV energy range using aligned crystals

A. Apyan,[1,*] R.O. Avakian,[1] B. Badelek,[2] S. Ballestrero,[3] C. Biino,[4,5] I. Birol,[6] P. Cenci,[7] S.H. Connell,[8] S. Eichblatt,[6] T. Fonseca,[6] A. Freund,[9] B. Gorini,[5] R. Groess,[8] K. Ispirian,[1] T.J. Ketel,[10] Yu.V. Kononets,[11] A. Lopez,[12] A. Mangiarotti,[3] B. van Rens,[10] J.P.F. Sellschop,[8,†] M. Shieh,[6] P. Sona,[3] V. Strakhovenko,[13] E. Uggerhøj,[14,‡] U.I. Uggerhøj,[15] G. Unel,[6] M. Velasco,[5,§] Z.Z. Vilakazi,[8,¶] and O. Wessely[2]

(The NA59 Collaboration)

[1] *Yerevan Physics Institute, Yerevan, Armenia*
[2] *Uppsala University, Uppsala, Sweden*
[3] *INFN and University of Firenze, Firenze, Italy*
[4] *INFN and University of Torino, Torino, Italy*
[5] *CERN, Geneva, Switzerland*
[6] *Northwestern University, Evanston, IL, USA*
[7] *INFN, Perugia, Italy*
[8] *Schonland Research Centre - University of the Witwatersrand, Johannesburg, South Africa*
[9] *ESRF, Grenoble, France*
[10] *NIKHEF, Amsterdam, The Netherlands*
[11] *Kurchatov Institute, Moscow, Russia*
[12] *University of Santiago de Compostela, Santiago de Compostela, Spain*
[13] *Institute of Nuclear Physics, Novosibirsk, Russia*
[14] *Institute for Storage Ring Facilities, University of Aarhus, Denmark*
[15] *University of Aarhus, Aarhus, Denmark*

(Dated: December 8, 2005)

The processes of coherent bremsstrahlung (CB) and coherent pair production (CPP) based on aligned crystal targets have been studied in the energy range 20-170 GeV. The experimental arrangement allowed these phenomena as well as their polarization dependence to be evaluated under conditions where single-photon cross-sections could be measured. This proved very important as the theoretical description of CB and CPP is an area of active theoretical debate and development. The theoretical approach used in this paper predicts both the cross sections and polarization observables very well for the experimental conditions investigated, indicating that the understanding of CB and CPP is reliable up to energies of 170 GeV. A birefringence effect in CPP was studied and it was demonstrated this enabled new technologies for high energy photon beam optics, such as polarimeters (for both linear and circular polarization) and phase plates. We also present new results regarding the features of coherent high energy photon emission for the Strings-Of-Strings (SOS) orientation, where the coherent enhancement of hard photon radiation is larger than for the CB case. The photon polarization in this case has been controversial. Our measurements commented on this situation as well.

PACS numbers: 03.65.Sq, 61.85.+p, 78.20.Fm, 78.70.-g, 95.75.Hi

I. INTRODUCTION

The demand for high energy circularly polarized photon beams has increased with the need to study gluon related features of the nucleon. The so-called "spin crisis of the nucleon" and its connection to the gluon polarization has attracted much attention [1]. For example, experiments to determine the gluon spin density of the nucleon [1, 2, 3] from polarized virtual photon-gluon fusion, and polarized virtual photoproduction of high transverse momentum mesons [4]. Future experiments will require intense high energy photon beams with a high degree of circular polarization. A well known method to produce circularly polarized photons is the interaction of longitudinally polarized electrons with crystalline media, where the emitted photons are circularly polarized due to conservation of angular momentum [5]. Specifically, theoretical calculations [6, 7] predict that the coherent bremsstrahlung (CB) and channeling radiation (CR) in crystals by longitudinally polarized electrons are also circularly polarized, and can be used to enhance the number of high energy circularly polarized photons. Currently, the highest energy available polarized electron beam is 45 GeV [8, 9]. Photons that will allow $\gamma g \to c\bar{c}$ in $\Lambda_c D$ production with a four-momentum fraction of the gluon of η have a threshold energy of $9.2/\eta$ GeV. Therefore, the available polarized electron beams cannot produce

*Now at: Northwestern University, Evanston, IL, USA
†Deceased
‡Co-Spokeperson
§Co-Spokeperson; Now at: Northwestern University, Evanston, IL, USA
¶Now at: University of Cape Town, Cape Town, South Africa

polarized photons that are sufficiently energetic, that is above 92 GeV, to investigate the gluon spin contribution to the proton by the above mentions reaction for η values of about 0.1.

Unpolarized electron beams are available to much higher energies, for example, energies of up to 250GeV at CERN and 125GeV at FNAL. Linearly polarized photons may be produced from such beams by CB. It is therefore of interest to investigate the possible conversion of this linear polarization to circular, and to develop polarimetry techniques at these very high photon energies. CB radiation differs from incoherent bremsstrahlung (ICB) in an amorphous target in that the cross section is substantially enhanced with relatively sharp peaks in the photon spectrum. The position of these peaks can be tuned by adjusting the electron beam incidence angle with respect to the major planes of the lattice. New features of coherent high energy photon emission develop at higher electron energies. For certain geometries for the incident electron beam with respect to the aligned crystal target so-called "strong field" become important. If the electron beam is incident very close to the plane (within the planar channeling critical angle) and also closely aligned to a major axis (but beyond the axial channeling critical angle), then the electrons interact dominantly with successive atomic strings in the plane. This orientation was aptly described by the term "string-of-strings" (SOS) by Lindhard, a pioneer of beam-crystal phenomena [10]. The polarization features of this SOS radiation require further investigation. In conclusion, a study of the above mentioned phenomena constitutes an opportunity to benchmark the latest theoretical approaches that describe CB and also the related process of CPP at these energies.

Accordingly, this paper has three distinct sections. The first section studies birefringent effects in CPP by photons in the 20-170 GeV energy range incident on aligned crystals. As a byproduct, a new crystal polarimetry technique is established. The second section extends the investigation of birefringence by aligned crystals and demonstrates the conversion of linear polarization to circular polarization for the CB photons. The crystal polarimetry technique is here extended to quantify also circular polarization. The third section addresses the issue of the polarization of SOS radiation. Also in this section it is demonstrated that the theory which is discussed accurately describes the observations. The theoretical calculations cover the cross sections for CB and SOS radiation for the photon generation, the cross section for CPP for the polarimetry, and the linear to circular polarization conversion. Simulations based on the theoretical calculations therefore predict the measured polarization observables. The good agreement between our measurements and the simulations indicate that, even for the strong field case, the theoretical description is reliable.

This work focuses both on cross sections and polarization phenomena in CB and CPP at high energies in oriented single crystals. The CB and CPP theories are constructed in the framework of the first Born approximation in the crystal potential. These theories are well established and were experimentally investigated for up to a few tens of GeV electrons and photons. The theoretical description of those phenomena in oriented single crystals becomes more complicated at higher energies. The processes have strong angular and energy dependence and the validity conditions of the Born approximation no longer hold at very high energies and small incidence angles with respect to the crystal axes and planes. The onset of this problem for the description of radiation emission and pair production (PP) has the characteristic angle $\theta_v = U_0/m$ [11] where U_0 is the plane potential well depth, m is the electron rest mass and $\hbar = c = 1$. The radiation and pair production processes can be described by the CB and CPP theory for the incidence angles with respect to the crystal axes/planes $\theta \gg \theta_v$. For angles $\theta \sim \theta_v$ and $\theta < \theta_v$ a different approach, known as the quasi classical description is used. In this approach the general theory of radiation and pair production is developed based on the quasi classical operator method [11].

II. PRODUCTION OF HIGH ENERGY PHOTON BEAMS

As described below, the so-called point effect (PE) orientation of the crystal was used in the first section of the experiment, where linear polarization studies of high energy CB photons were performed and birefringent effects in pair production on aligned crystals were studied. This section of the experiment also leads to a new polarimetry technique [12].

The same orientation was also used in the second section of the experiment, where the conversion of the linear polarization to circular polarization induced by a birefringent effect in an aligned single crystal was studied [13].

For the third section of the experiment, the crystal orientation appropriate for SOS radiation was used [14]. This radiation production scenario is also treated below.

A. Linearly polarized CB photons

In the production of photon beams, single crystals can play an important role by exploiting coherent and strong field effects that arise for oriented incidence in the interaction of radiation and matter in crystalline materials [15]. The CB method is a well established technique for obtaining linearly polarized photons starting from unpolarized electrons [16, 17, 18, 19]. An electron impinging on a crystal will interact coherently with the electric fields of the atoms in aligned crystal planes. If the Laue condition is satisfied, the bremsstrahlung photons will be emitted at specific energies corresponding to the selected vectors of the reciprocal lattice. In the so-called PE orientation of the crystal the direction of the electron

beam has a small angle with respect to a chosen crystallographic plane and a relatively large angle with the crystallographic axes that are in that plane. For this PE orientation of the single crystal only one reciprocal lattice vector contributes to the CB cross section. The CB radiation from a crystal aligned in this configuration is more intense than the ICB radiation in amorphous media and a high degree of linear polarization can be achieved [17]. The maximum polarization and the maximum peak intensity occur at the same photon energy, and this energy can be selected by choosing the orientation of the lattice planes with respect to the incoming electron beam. This property has been used previously to achieve photon beams with up to 70% linear polarization starting from 6 GeV electrons [20], and up to 60% linear polarization starting from 80 GeV electrons [21].

The emission mechanism of the high energy photons is CB connected to the periodic structure of the crystal [17]. The peak energy of the CB photons, E_γ, is determined from the condition (the system of units used here has $\hbar = \mathrm{c} = 1$),

$$\frac{1}{|q_\parallel|} = 2\lambda_c\gamma\frac{E_0 - E_\gamma}{E_\gamma} \ , \qquad (1)$$

where $|q_\parallel|$ is the component of the recoil momentum of the nucleus parallel to the initial electron velocity and the other symbols have their usual meanings. Recall, in a crystal possible values of $\mathbf{q}$, from which the contribution to the coherent radiation comes, are discrete: $\mathbf{q} = \mathbf{g}$ [17], where $\mathbf{g}$ is a reciprocal lattice vector of the crystal. The minimal reciprocal lattice vector giving rise to the main CB peak is given by

$$|g_\parallel|_{min} = \frac{2\pi}{d}\Theta. \qquad (2)$$

For the PE orientation, d is the interplanar distance and $\Theta = \psi$, the electron incident angle with respect to the plane.

The position of the hard photon peak can be selected by simultaneous solution of the last two equations

$$\Theta = \frac{d}{4\pi\gamma\lambda_c}\frac{E_\gamma}{E_0 - E_\gamma}. \qquad (3)$$

The coherence length determines the effective longitudinal dimension of the interaction region for the phase coherence of the radiation process:

$$l_{coh} = \frac{1}{|q_\parallel|}. \qquad (4)$$

The relative merits of different single crystals as CB radiators have been investigated in the past [22]. The silicon crystal stands out as a good choice due to its availability, ease of growth, and low mosaic spread. A Si crystal thickness of 1.5 cm was selected to achieve a relatively low photon multiplicity and reasonable photon emission rate. This multiplicity is shown in Fig. 1 to reside dominantly in lower energy photons.

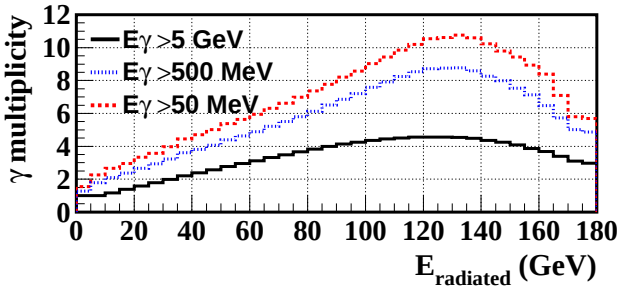

FIG. 1: MC prediction for photon multiplicity vs total radiated energy using different photon energy cut-off values.

For an 178 GeV electron beam making an angle of 5 mrad from the <001> crystallographic axis and about 70 μrad from the (110) plane, the resulting photon beam polarization spectrum was predicted to yield maximum polarization of about 55% in the vicinity of 70 GeV, as seen in Fig. 2.

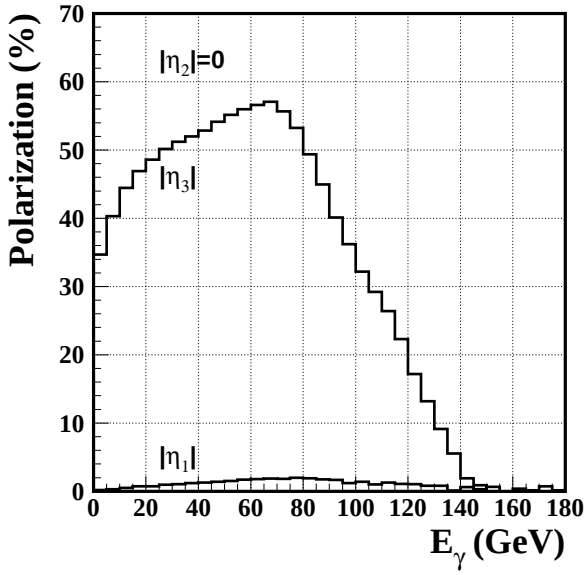

FIG. 2: Expected Polarization for NA59 photon beam.

For this choice of crystal orientation the incidence angles of electrons and photons to the crystal plane become comparable with the radiation and pair production characteristic angle θ_v. In case of the (110) plane of the silicon crystal, we find θ_v=42 μrad. In fact part of the incident electron beam penetrates the crystal with angles both less and greater than θ_v, because of the angular divergence of the electron beam. In the theoretical simulations presented here, a Monte Carlo approach was used to model the divergence of the electron and photon beams, and the relevant theories (CB and CPP or the quasi classical theory) are selected as appropriate for accurate and fast calculation. It will be shown later that this approach has lead to a very good agreement between the theoretical

predictions and the data.

B. Enhanced production of SOS photons

The character of the radiation, including its linear polarization, is changed when the direction of the electron (i) has a small angle with a crystallographic axis and (ii) is parallel with the plane that is formed by the atomic strings along the chosen axes. This is the so-called SOS orientation. It produces a harder photon spectrum than the CB case because the coherent radiation arises from successive scattering off the axial potential, which is deeper than the planar potential. The radiation phenomena in single crystals aligned in SOS mode have been under active theoretical investigation since the NA43 collaboration discovered, for the first time, two distinct photon peaks, one in the low energy region and one in the high energy region of the radiated energy spectrum for about 150 GeV electrons traversing a diamond crystal [23]. It was established that the hard photon peak was a single photon peak [15]. However, the radiated photons were generally emitted with significant multiplicity in such a way that a hard photon would be accompanied by a few low energy photons. It will be seen later that two different mechanisms are responsible for the soft and the hard photons. In the former case, it is planar channeling (PC) radiation, while in the latter case, it is SOS radiation. An additional intriguing feature of SOS radiation at these energies ($E_\gamma \approx 120$ GeV) is that it occurs at the onset of a regime where strong field effects need to be taken into account. These fields are characterised by the parameter $\chi = \gamma\mathcal{E}/\mathcal{E}_0$ where $\gamma\mathcal{E}$ is the boosted crystal field in the electron frame and $\mathcal{E}_0$ is the Schwinger field. This is defined as the field which separates a virtual pair by the electron Compton wavelength, $\mathcal{E}_0 = m/e\lambda_c$ [24, 25, 26]. The quantum suppression of radiation expected under these conditions [11, 27, 28] was evidenced [15, 29, 30]. Other situations where such conditions have been achieved are terawatt laser fields and above barrier very heavy ion collisions.

The issue of the polarization of SOS radiation also came into question. Early experiments with electron beams of up to 10 GeV in single crystals showed a smaller linear polarization of the more intense radiation in the SOS orientation than in the PE orientation (see [31] and references therein). The first measurements of linear polarization for high energy photons ($E_\gamma \approx 50 - 150$ GeV) were consistent with a high degree of linear polarization of the radiated photons [32]. At this stage the theoretical prediction of the SOS hard photon polarization was unresolved. It was however clear that the photons emitted by the PC mechanism would be linearly polarized. The polarimeter in this experiment recorded the integral polarization for a given radiated energy, which was likely to have a multi-photon character. This experiment therefore could not be considered conclusive as it did not separate the PC and SOS components and the extent to which pile-up from the low energy photons perturbed the high energy part of the total radiated energy spectrum was not resolved. These results therefore required more theoretical and experimental investigation.

A theory of photon emission by electrons along the SOS orientation of single crystals has since been developed. The theory takes into account the change of the effective electron mass in the fields due to the crystallographic planes and the crossing of the atomic strings [33]. The authors show that the SOS specific potential affects the high energy photon emission and also gives an additional contribution in the low energy region of the spectrum. In references [34, 35] the linear polarization of the emitted photons was derived and analysed for different beam energies and crystal orientations. The predicted linear polarization of hard photons produced using the SOS orientation of the crystal is small compared to the comparable case using the PE orientation of the crystal. On the other hand, the additional soft photons produced with SOS orientation of the crystal are predicted to exhibit a high degree of polarization.

The peak energy of the SOS photons, E_γ, is determined from the same condition as for CP photons (equation 1). However, for the SOS orientation, d is the spacing between the axes (strings) forming the planes, and $\Theta = \theta$, the electron incident angle with respect to the axis.

With the appropriate choice of θ the intensity of the SOS radiation may exceed the Bethe-Heitler radiation (incoherent bremsstrahlung (ICB)) by an order of magnitude.

When a thin silicon crystal is used with an electron beam of energy $E_0 = 178$ GeV incident along the SOS orientation, within the (110) plane and with an angle of $\theta = 0.3$ mrad to the $< 100 >$ axis, the hard photon peak position is expected at $E_\gamma = 129$ GeV.

In the current experiment, a 1.5 cm thick silicon crystal was used in the SOS orientation as mentioned above. Under this condition the radiation is expected to be enhanced by about a factor 20 with respect to the ICB for a randomly oriented crystalline Si target of the same thickness.

The radiation spectrum with the crystal aligned in SOS orientation has in addition to the CB radiation a strong component at a low energy which is characteristic of planar channelling (PC) radiation. As the electron direction lines up with a crystallographic plane in the SOS orientation, the planar channelling condition is fulfilled. For channelling radiation the coherence length is much longer than the interatomic distances and the long range motion, characteristic of planar channelled electrons, becomes dominant over short range variations with the emission of low energy photons. Theoretical calculations [36, 37] predict a more intense soft photon contribution (PC) with a high degree of linear polarization of up to 70%.

The calculations of the enhancements of both the low energy and the high energy components of the radiation emission for the SOS orientation under conditions appli-

cable to this experiment are presented in Fig. 3. Where $E_0 = 178\,\text{GeV}$ electron beam incidences the (110) plane and at an angle of $\theta = 0.3\,\text{mrad}$ to the $\langle 100 \rangle$ axis. At low energy the PC radiation dominates and at high energies the SOS radiation peaks.

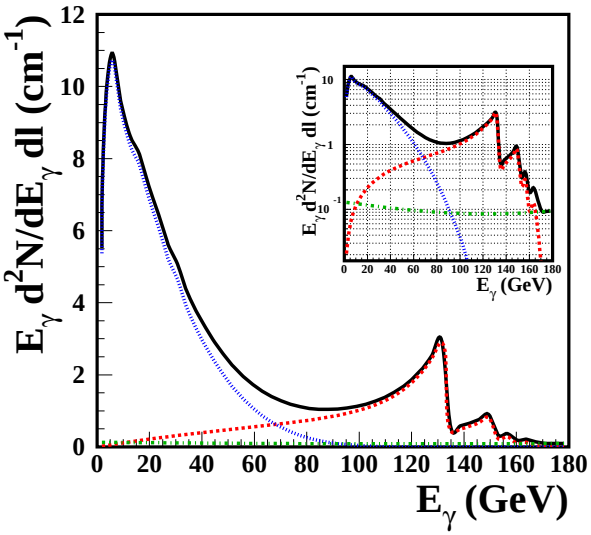

FIG. 3: Photon power yield, $E_\gamma d^2N/dE_\gamma dl$, per unit of thickness for a thin silicon crystal in the SOS orientation. The solid curve represents the total of the contributions from ICB (green dash-dotted), PC (blue dotted) and SOS (red dashed) radiation. The insert is a logarithmic representation and shows the flat incoherent contribution and the enhancement with a factor of about 20 for SOS radiation at 129 GeV.

III. BEAM OPTIC ELEMENTS FOR VERY HIGH ENERGY PHOTON BEAMS

In this work the polarization observables for high energy photons produced either by CB or SOS radiation are determined using the birefringence phenomena in CPP on aligned crystals. The study of the conversion of linear to circular polarization is based on the same birefringent effect in CPP. The experiments and their theoretical simulation therefore represent simultaneously a test of the theoretical understanding as well as development of new beam-optic elements based on crystal techniques.

A. Birefringence in CPP and crystal polarimetry

Historically, the pair conversion in single crystals was proposed, and later successfully used in the 1960s as a method to measure linear polarization for photons in the 1-6 GeV range [38]. It was predicted theoretically and later verified experimentally [39] that the pair production cross section and the sensitivity to photon polarization increases with increasing energy. Therefore, at sufficiently high photon energies, a new polarization technique based on this effect can be constructed, which will become competitiveto other techniques, such as pair production in amorphous media and photo nuclear methods.

In the first part of the experiment, the cross section for CPP by polarized photons incident on the aligned "analyzer" crystals (germanium and diamond) was measured, for different carefully selected crystallographic orientations. This process can be effectively viewed as the imaginary part of the refractive index, as it leads to an attenuation of the photon beam. It constitutes a birefringence phenomenon, as the imaginary part of the refractive index will differ as a function of the angle between the plane of polarization of the photon beam and a specific crystallographic orientation of the "analyzer" crystal. A polarimeter was constructed by measuring the energy dependent asymmetry with respect to the two most distinct orientations of the analyzer crystal for pair production.

The theoretical comparison to the data could validate the calculation of the energy dependence of the cross section and the polarization of photons produced by coherent bremsstrahlung as well as the calculation of coherent pair production for polarized photons incident on crystals of different crystallographic orientations.

The photon polarization is expressed using the Stoke's parametrisation with the Landau convention, where the total elliptical polarization is decomposed into two independent linear components and a circular component. Referred to our geometry the parameter η_1 describes the linear polarization of the beam polarized in the direction of 45° to the reaction plane of the radiator, while the parameter η_3 describes the linear polarization in the direction parallel or perpendicular to the reaction plane of the radiator. The parameter η_2 describes the circular polarization. The total polarization is then written:

$$P_{\text{linear}} = \sqrt{\eta_1^2 + \eta_3^2}, \quad P_{\text{circular}} = \sqrt{\eta_2^2}, \quad P_{\text{total}} = \sqrt{P_{\text{linear}}^2 + P_{\text{circular}}^2} \quad . \tag{5}$$

The radiator angular settings were chosen to have the total linear polarization from CB radiation purely along η_3. Two distinct measurements were made, one to show that the η_1 component of the polarization was consistent

with zero and another to find the expected η_3 component of polarization as shown in Fig. 2. The MC calculations used to obtain this prediction took into account the divergence of the electron beam (48 μrad horizontally and 33 μrad vertically) and the 1% uncertainty in its 178 GeV energy. To optimise the processing time of the MC simulation, minimum energy cuts of 5 GeV for the electrons and 500 MeV for the photons were applied. We were, therefore, able to predict both the total radiated energy spectrum and the energy spectrum of individual photons.

The polarization dependence of the pair production cross section and the birefringent properties of crystals are key elements of the photon polarization measurement. The imaginary parts of the refraction indices are related to the pair production cross section. This cross section is sensitive to the relative angle between a crystal plane of a specific symmetry and the plane of linear polarization of the incident photon. In essence, the two orthogonal directions where these two planes are either parallel or perpendicular to each other yield the greatest difference in pair production cross section.

Thus, the dependence of the CPP cross section on the linear polarization of the photon beam makes an oriented single crystal suitable as an efficient polarimeter for high energy photons. The existence of a strong anisotropy for the production of the e^+e^- pairs during their formation is the reason for the polarization dependent CPP cross section of photons passing through oriented crystals. This means that perfect alignment along a crystallographic axis is not an efficient analyzer orientation due to the approximate cylindrical symmetry of the crystal around atomic strings. However, for small angles of the photon beam with respect to the crystallographic symmetry directions the conditions for the formation of the e^+e^- pairs prove to be very anisotropic. As it turns out, the orientations with the highest analyzing power are those where the e^+e^- pair formation zone is not only highly anisotropic but also inhomogeneous with maximal fluctuations of the crystal potential along the electron path. At the crystallographic axes the potential is largest and so are the fluctuations. These conditions are related to the ones of the SOS orientation: (i) a small angle to a crystallographic axis to enhance the pair production process by the large fluctuations and (ii) a smaller angle to the crystallographic plane to have a long but still anisotropic formation zone for CPP.

We therefore studied the pairs created in a second aligned crystal, called the *analyzer* crystal. In this study, the experimentally relevant quantity is the asymmetry, A, between the pair production cross sections, σ, of parallel and perpendicular polarized photons, where the polarization direction is measured with respect to the <110> crystallographic plane of the analyzer crystal. This asymmetry is related to the linear photon polarization, P_1, through the equation

$$A \equiv \frac{\sigma(\gamma_\perp \to e^+e^-) - \sigma(\gamma_\parallel \to e^+e^-)}{\sigma(\gamma_\perp \to e^+e^-) + \sigma(\gamma_\parallel \to e^+e^-)} = R \times P_1. \quad (6)$$

Here R is the so called "analysing power" of the second crystal. The analysing power is in fact the asymmetry expected for a 100% linearly polarized photon beam. It will be seen that for the conditions of this experiment, and using the theory described, this quantity can be reliably computed using Monte Carlo simulations. In this polarimetry method, the crystal with the highest possible analysing power is preferred in order to achieve a fast determination of the photon polarization.

If one defines the ratio of the energy of one of the pairs, E^-, to the energy of the incoming photon, E_γ, as

$$y \equiv E^-/E_\gamma \quad , \quad (7)$$

then one may calculate the dependence of the pair production rate on this ratio, y, as shown in Fig. 4.

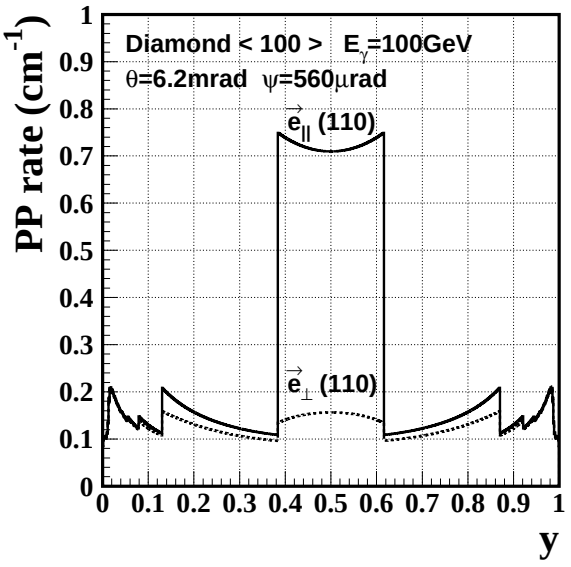

FIG. 4: Pair production rate vs the pair asymmetry, y, as defined in the text.

By comparing the rates for the photon polarization parallel (solid line) and perpendicular (dashed line) to the crystallographic plane, we observe that the largest difference arises for $0.4 \leq y \leq 0.6$. Therefore the pair production asymmetry may be maximised by selecting the subset of events where the e^+e^- pairs have similar energies. This method of choosing the pairs to enhance the analysing power is called the "quasi-symmetrical pair selection method" [40]. As a result of such a cut, although the total number of events decreases, the relative statistical error diminishes since it is inversely correlated with the measured asymmetry. If the efficiencies of the pair events and beam intensity normalisation events are assumed to be the same, then the cross section measurement in equation (6) reduces to counting these events separately. Denoting the number of pairs produced in perpendicular and parallel cases by p_1 and p_2, and the

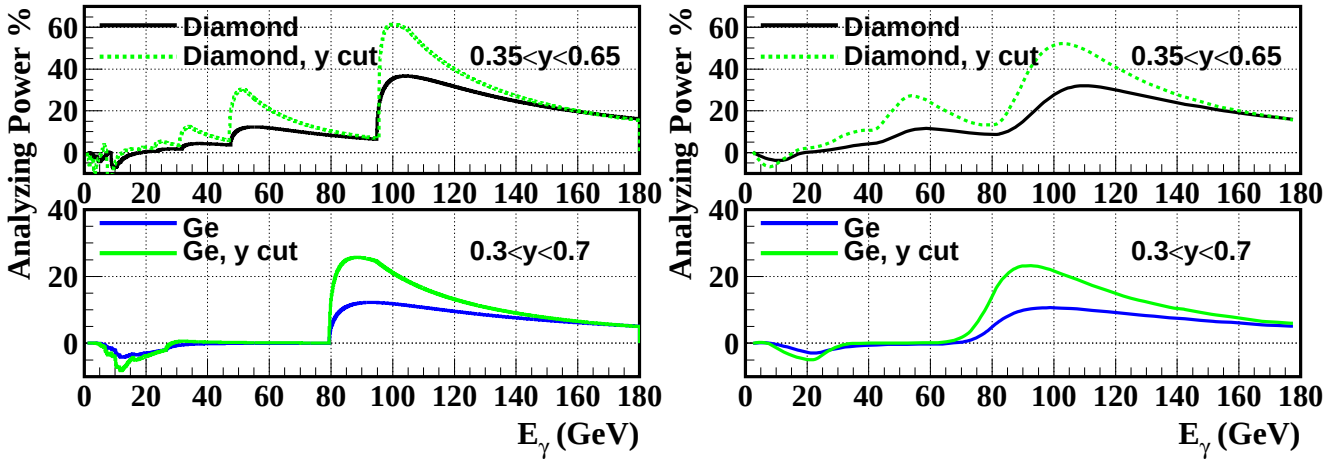

FIG. 5: Analysing power of different single crystals, for an ideal e^- beam without any angular divergences (left) and for NA59 e^- beam conditions (right).

number of the normalisation events in each case by n_1 and n_2, respectively, the measured asymmetry can be written as:

$$A = \frac{p_1/n_1 - p_2/n_2}{p_1/n_1 + p_2/n_2}, \tag{8}$$

where p and n are acquired simultaneously and therefore are correlated.

1. *Germanium and diamond analyzer crystals*

The first analyzer crystal used in the NA59 experiment was a germanium (Ge) single crystal disk with a diameter of 3 cm and a thickness of 1.0 mm. The selected orientation with respect to the incident photon beam represented a polar angle of 3.0 mrad measured from the <110> axis and an azimuthal anglecorresponding to incidence exactly on the $(1\bar{1}0)$ plane. This configuration gave an analysing power peaking at 90 GeV, as can be seen in Fig. 5. From the same figure one can also see that the quasi-symmetrical pair selection method delivers almost twice the analysing power. The same single Ge crystal had also been used in the a previous experiment, NA43. The pair production properties of this thickness of germanium crystal are therefore well known [41].

The second analyzer of the NA59 experiment was a multi-tile synthetic diamond crystal target with an incident photon beam orientation with respect to the crystal of 6.2 mrad from the <100> axis and 560 μrad from the (110) plane.

The major advantage of using diamond in the analyzer role are its high pair yield, high analysing power (see Fig. 5) and radiation hardness. The photon beam dimensions of NA59 implied that one would need a diamond with an area of about 20mm×20mm. A crystal thickness of 4 mm was a fair compromise between requirements of the Figure of Merit (FOM) for a diamond analyzer and the costs of the material. These requirements were realised by developing a composite target comprising of four synthetic diamonds of dimensions $8\times8\times4$ mm^3 arranged in a square lattice as seen in Fig. 6.

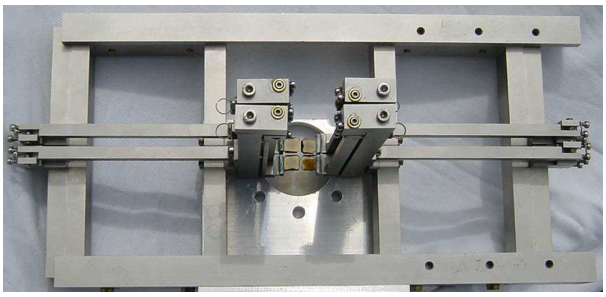

FIG. 6: The diamond analyzer target consists of synthetic diamond tiles and the aluminium holder frame.

Selected areas of synthetic diamonds grown under conditions of high pressure and temperature using the "reconstitution" technique [42] and other proprietary procedures exhibit crystal structures superior to high quality natural samples. A long term program of studying large synthetic single diamond crystals using X-ray diffraction rocking curve widths, X-ray topography [43, 44], cathodo-luminescence and indeed, experiments with coherent bremsstrahlung and pair production in experiment NA43 on a range of diamonds informed this procedure. The four diamonds used in the composite analyzer target were therefore extracted from chosen regions of selected synthetic material yielding regular tiles with optical surface finishes. The tiles had been polished with faces corresponding to cubic directions with an accuracy of about 0.2 degrees using Laue back-reflection photographs. This pre-alignment fell short of the requirements of the experiment. Each diamond tile should be

mutually aligned with its neighbours so that the <100> axes normal to the tile (approximately the beam direction) corresponded within 5 μrad. In addition, the mutual azimuthal alignment of the crystallographic axes in the plane of the tile surfaces should be within 200 μrad.

Accordingly, a mechanical system that featured three rotational degrees of freedom for each diamond tile was designed. This rotation was effected by mounting the diamond tiles on lever arms attached to a rigid frame using spring loaded flexure hinges which could be actuated by very fine threaded screws with significant mechanical advantage. Since the outer dimensions of the whole four-crystal system were limited to 300 x 150 mm we had to constrain the lengths of the lever arms to about 100 mm. The dynamic range in angle space of the lever arms was necessarilylimited, requiring the diamond tiles to be pre-aligned in the adhesion mounting process. This was achieved using a goniometer mounted vacuum tweezer to offer the tile to the lever arm during fixing, under conditions of monitoring the crystallographic orientation using an X-ray system. The adhesive used was dental cement and the inter tile separation was 1 mm. The final accurate mutual alignment was performed on a precise X-ray diffractometer at CNRS, Grenoble/France using a well-collimated pencil beam. The whole alignment system shown in Fig. 6 was mounted on a high precision XY-translation table allowing each of the four crystals to be illuminated with the pencil X-ray beam in turn. The slopes of the Bragg peak at half maximum were used rather than the peak centre, as greater sensitivity could be achieved in this way. This procedure was repeated several times for all crystals to make sure that any cross-correlations between the angular rotations were eliminated. Ultimately, all lever arms were locked in position with dental cement to avoid any loss of the adjustment by vibrations during transport from Grenoble to CERN.

This last procedure corresponded to the mutual alignment between the elements of the composite target. The procedure was considered effective and can form the basis of future aligned composite target systems.

An additional fine alignment is necessary in the orientation of radiator crystal (Coherent Bremsstrahlung) and the analyzer crystal (Asymmetry in Pair Production for two orthogonal analyzer crystal orientations) with the ideal particle in the beam envelope.

The initial transfer of alignment from the X-Ray pre-alignment system to the goniometer systems of the photon beam-line was affected either through a correspondence in the mechanical mounting systems. In some cases an optical laser reflection which had been calibrated in the course of the X-ray pre-alignment process was also used.

Once beam was available, the fine alignment was performed (and indeed regularly controlled during the experiment). A narrow electron beam was directed onto the crystal, and data was collected using the minimum bias trigger. A scan of the incident angular phase space between the beam and the crystal was performed by programming the motion of the crystal mounted in the goniometers. The crystallographic axes and planes could be identified as positions in this phase space where the coherent enhancements (or reductions) of a radiation phenomenon in relation to the corresponded incoherent cross-section occurred. This would be observed in an appropriate detector.

The radiator crystal was therefore aligned exploiting the physics of bremsstrahlung from the electron beam as observed in the Lead Glass Calorimeter. On the other hand, the analyzer crystal was aligned by observing pair-production by the photon beam generated in the radiator crystal as observed in the multiplicity counter.

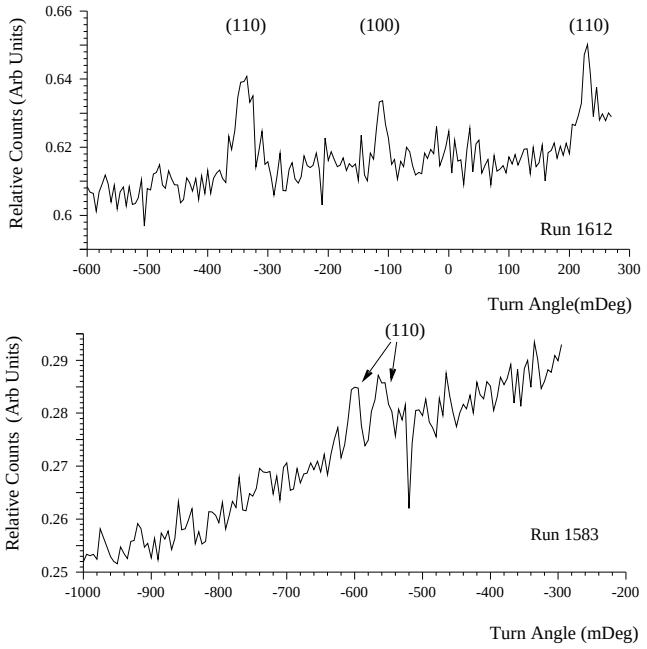

FIG. 7: TOP: Scanning across the incident angle phase space between the beam and the crystal reveals coherent enhancements of the pair-production cross-section due to planar effects, as the planes are traversed in the scan. Stereograms generated from many orthogonal scans in the region around the axis allows the identification of the crystallographic planes. BOTTOM: The mapping of the crystallographic planes revealed a misaligned tile. The misaligned tile was identified in the offline analysis.

Stereograms of the coherent enhancements were plotted in the incident angle phase space. This allowed the planes around the axis to be accurately identified and tracked. Usually, one would explore the region around the axis, but off the axis, and then extrapolate the position of the axis using the well understood and recognised behaviour of the surrounding planes.

During the fine alignment process for the compound diamond target (Fig. 7), it was observed that one of the tiles of the multi-crystal diamond analyzer was accidentally misaligned. This lead to a "doublet" when one scanned across a plane. Analysis of the stereogram

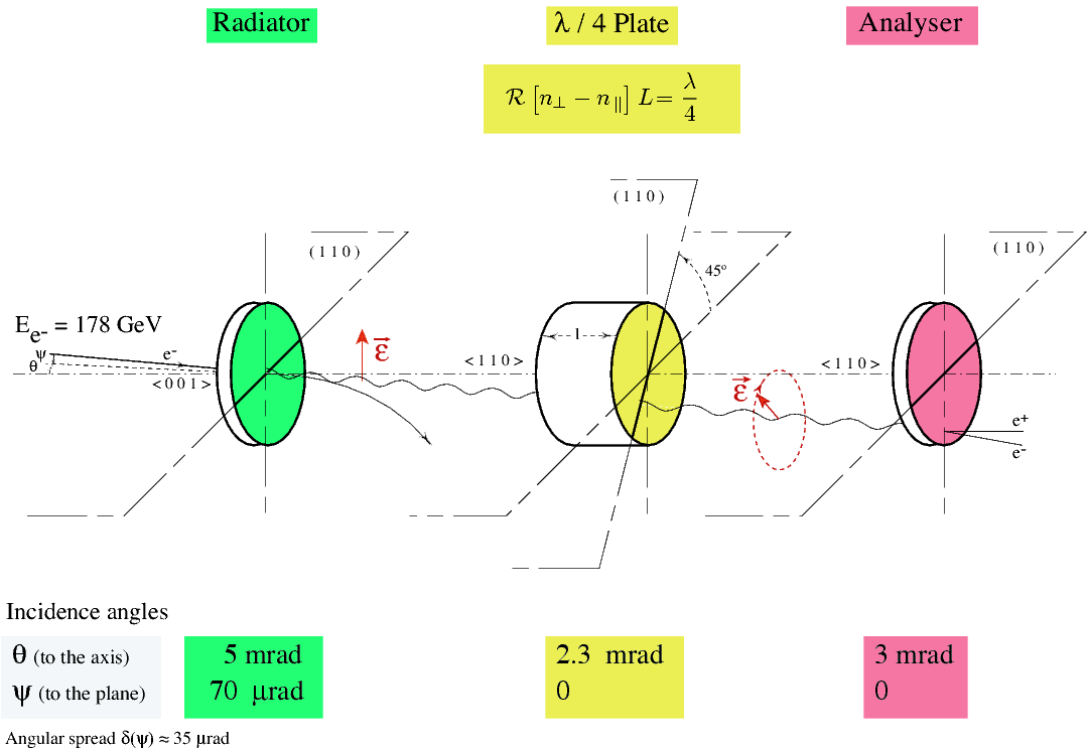

FIG. 8: Three crystal scheme.

indicated that one of the diamonds was out of alignment by 2.1 degrees (bottom of Fig. 7). This effect was incorporated in the offline analysis where separate spectra for each diamond of the multi-diamond target could be achieved.The offending tile was identified and excluded from the analysis.

B. Conversion of linear to circular polarization

The second section of the experiment tested the feasibility of producing circularly polarized photon beams in proton accelerators using the extracted unpolarized high energy electron beams (for example, with energies of up to 250 GeV (CERN) and 125 GeV (FNAL) [45]). These unpolarized electron beams can produce linearly polarized photons via CB radiation in an aligned single crystal. One can transform the initial linear polarization into circular polarization by using the birefringent properties of aligned crystals. The above mentioned method was first proposed by Cabibbo and collaborators in the 1960's [46], and later the numerical calculations were done in terms of CPP theory [17] to obtain the optimal thicknesses for various cubic crystals. To perform the experimental investigation, a consecutive arrangement of three aligned single crystals was used. The first crystal acted as a radiator to produce a linearly polarized photon beam, the second crystal acted as a quarter wave plate to convert the linear polarization into circular polarization, and the last crystal acted as an analyzer to measure the change in the linear polarization of the photon beam. The three-crystal scheme used is shown in Fig. 8.

The linearly polarized photon beam was produced by CB radiation from electrons in an aligned Si <100> single crystal, as already described above (section II A). For the conversion of the linear polarization into circular polarization an aligned Si <110> crystal was used. Finally the aligned Ge<110> crystal was used as an *analyzer* of the linear polarization of photon beam, also as discussed above (section III A).

When high energy photon beam propagates through a medium, the main process by which the photons are absorbed is e^+e^- pair production. When photons propagate through an aligned crystal at small incident angles with respect to a crystal axis and/or a crystal plane, a coherent enhancement of the PP is manifested (CPP). The cross section for the CPP process depends on the direction of the linear polarization of the photon beam with respect to the crystal axis and to the photon momentum (reaction plane) as shown in Fig. 8. Generally speaking, one can represent the linear polarization of the photon beam as a superposition of two beams with polarization directions parallel and perpendicular to the reaction plane containing the photon momentum $\boldsymbol{k}$ and the crystallographic axis. In this case, the photon polarization vector $\boldsymbol{e}$ will be the combination of two unit vectors, $\boldsymbol{t}$ and $\boldsymbol{y}$, parallel and perpendicular to the reaction plane, respectively:

$$\boldsymbol{e} = e_{\parallel}\boldsymbol{t} + e_{\perp}\boldsymbol{y}. \quad (9)$$

The components of the polarization vector before and after the crystal of thickness, L, are related by a 2×2 matrix [46, 47]:

$$\begin{pmatrix} e_{\parallel}(L) \\ e_{\perp}(L) \end{pmatrix} = \begin{pmatrix} \exp[in_{\parallel}E_{\gamma}L] & 0 \\ 0 & \exp[in_{\perp}E_{\gamma}L] \end{pmatrix} \begin{pmatrix} e_{\parallel}(0) \\ e_{\perp}(0) \end{pmatrix}$$

where E_{γ}=$|\boldsymbol{k}|$ ($\hbar = c = 1$) is the energy of the incident photon and the $n_{\parallel}$ and $n_{\perp}$ are complex quantities analogous to the index of refraction. The imaginary part of the index of refraction is connected with the photon absorption cross section, while the real part can be derived from the imaginary part using dispersion relations [46]. The crystal can act as a *quarter wave plate*, if the real part of the relative phases of the two components of the waves parallel and perpendicular to the reaction plane is changed by $\pi/2$ after transmission of the photon. Thus the crystal will be able to transform the linear polarization of the photon beam into circular polarization at the matching thickness:

$$L = \frac{2}{\pi}\frac{1}{E_{\gamma}\Re(n_{\perp} - n_{\parallel})}. \quad (10)$$

The polarization is expressed again as in section III A. The photon beam intensity and Stokes parameters after the quarter wave plate with the thickness L can be derived from the following formulae [11]:

$$\begin{aligned} N(L) &= N(0)[\cosh aL + \eta_1 \sinh aL]\exp(-WL), \\ \eta_1(L) &= \frac{\sinh aL + \eta_1(0)\cosh aL}{\cosh aL + \eta_1(0)\sinh aL}, \\ \eta_2(L) &= -\frac{\eta_3(0)\sin bL - \eta_2(0)\cos bL}{\cosh aL + \eta_1(0)\sinh aL}, \\ \eta_3(L) &= -\frac{\eta_3(0)\cos bL + \eta_2(0)\sin bL}{\cosh aL + \eta_1(0)\sinh aL}, \end{aligned} \quad (11)$$

with

$$\begin{aligned} a &= E_{\gamma}\Im(n_{\perp} - n_{\parallel}) = \frac{1}{2}(W_{\parallel} - W_{\perp}), \\ b &= E_{\gamma}\Re(n_{\perp} - n_{\parallel}), \quad W = \frac{1}{2}(W_{\parallel} + W_{\perp}), \end{aligned} \quad (12)$$

where $W_{\parallel}$ and $W_{\perp}$ are the pair production probabilities per unit path length for photons polarized parallel or perpendicular to the reaction plane, respectively.

As follows from equation (11), the component of the linear polarization in the direction of 45° to the reaction plane of the quarter wave crystal is transformed into circular polarization [11]. Therefore the *quarter wave plate* should be rotated by 45° with respect to the polar plane of the photon beam to have the optimal transformation of the polarization. In this case the linear polarization component η_3, which was defined as the one parallel or perpendicular to the reaction plane of the radiator, represents a component of the linear polarization in the direction of 45° to the reaction plane of the quarter wave plate equation (11).

As follows from equation (11), the total polarization of the photon beam before and after the quarter wave crystal are connected by the relation:

$$P^2_{total}(L) = 1 + \frac{P^2_{total}(0) - 1}{(\cosh aL + \eta_1(0)\sinh aL)^2}. \quad (13)$$

There is conservation of polarization if the incident photon beam is completely polarized. In a real experiment, the incident photon beam is not completely polarized, and one must seek an alternative conserved quantity. Further study of equation (11) reveals that the quantity

$$K \equiv \frac{\eta_2^2(\ell) + \eta_3^2(\ell)}{1 - \eta_1^2(\ell)} \quad (14)$$

is constant and conserved when a photon beam penetrates the quarter wave plate crystal [48]. This relation holds for any penetration length, ℓ, between $0 \leq \ell \leq L$ except in the case when $\eta_2(0) = \eta_3(0) \equiv 0$ and $\eta_1(0) = 1$. It allows the determination of the resulting circular polarization of photon beam by measuring its linear polarization before and after the quarter wave plate. Taking into account the experimental condition, i.e. the photon beam angular divergences, one can note that K is conserved with ≈5% accuracy in the 80-110 GeV region as show Monte-Carlo simulations.

Fig. 9 shows the expected dependence of the Stokes parameters describing the photon polarization as a function of the *quarter wave plate* thickness, ℓ, for the surviving photons from a beam of 100 GeV. One can see that the initial total polarization is not conserved in the case of a partially polarized photon beam as expected from equation (13), nevertheless, the relation (13) still holds.

These calculations were carried out assuming that the Stokes parameters before the *quarter wave plate* had the following values: η_1=0.01, η_2=0 and η_3=0.36. In Fig. 9 (left), the photon beam makes an angle θ_0=2.3 mrad with respect to the <110> axis and lies in the (110) plane (ψ=0), while in Fig. 9 (right), the photon beam traverses the (110) plane at a small angle, ψ=±40 μrad.

One can see the increase in the total polarization, P_{total}, after the *quarter wave plate* with respect to the initial total polarization (the straight line around 0.36). This difference comes from the fact that the aligned *quarter wave plate* can also act as a polarizer. Therefore, the total polarization behind the *quarter wave plate* can be higher than the initial polarization. This increase is more pronounced in the case when the photon momentum makes a small angle of ψ=40 μrad with respect to the

crystal plane (Fig. 9 right). As described in section IV A and as shown in Fig. 21, the final calculation takes into account the beam divergence, in both the horizontal and vertical planes.

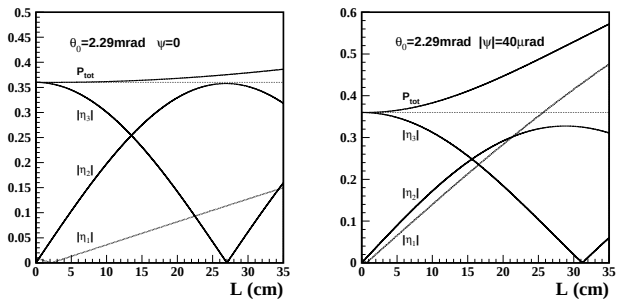

FIG. 9: Absolute values of the Stokes parameters and the total degree of polarization for a Si crystal as a function of its thickness L, for E_γ=100 GeV linearly polarized photons. The left hand figure and the right hand figure are calculated using initial values for the Stokes parameters described in the text. For these conditions, the crystal also acts as polarizer generating a η_1 component.

As seen from figure 9 the Si crystal with a thickness of $L >$25cm can act as a quarter wave plate taking into account the angular divergence of the γ-beam. For these crystal thicknesses where the $\eta_3(0)$ component of the initial linear photon beam polarization will be totally transformed into the final circular component $\eta_2(L)$, only a few percent of the photons will survive. We defined a FOM, to find a compromise between the photon beam attenuation and the polarization transformation efficiency in [45], as:

$$FOM = \eta_2(\ell)\sqrt{N(\ell)}. \tag{15}$$

Here $N(\ell)$ is the statistical weight of the number of surviving photons. Taking into account equation (15), references [49, 50, 51] presented theoretical predictions showing the possibility of transforming the linear polarization of a high energy photon beam into circular polarization in the 70-100 GeV energy range. The theoretical calculations of the energy and the orientation dependence of the indices of refraction were performed using the quasi-classical operator method and CPP formulae respectively. In both these references, the optimum thickness for a *quarter wave plate* Si crystal was found to be 10 cm. The relevant geometrical parameters involved the photon beam forming an angle of 2.29 mrad from the axis (110) and the photon momentum directly in the (110) plane of Si single crystal, *i.e.* the angle between the photon momentum and crystal plane is ψ=0. For this choice of parameters, the fraction of surviving photons is 17-20%.

C. SOS radiation

For the production of the much enhanced yield of the SOS photons as compared to the CB photons, the first radiator crystal was adjusted to appropriate angle settings. These were a beam angle of $\theta = 0.3$ mrad to the $\langle 100 \rangle$ axis in the (110) plane of the 1.5 cm thick Si crystal which is the optimal angle for a high energy SOS photon peak at 129 GeV (see Fig. 3) energy photon peak with a thin radiator at 125 GeV (see Fig. 3). As has been mentioned in section II B, the radiation probability with a thin radiator is expected to be 20 times larger at that energy than the Bethe-Heitler (ICB) prediction for randomly oriented crystalline Si.

The polarization measurements were then performed in a similar way to those of section III A for the analysis of linear polarization in CB radiation.

IV. EXPERIMENT AND ANALYSIS

The NA59 experiment was performed in the North Area of the CERN SPS, where unpolarized electron beams with energies above 100 GeV are available. We used a beam of 178 GeV electrons with angular divergence of $\sigma_{x'} = 48$ μrad and $\sigma_{y'} = 35$ μrad in the horizontal and vertical plane, respectively.

A. The Setup

The experimental setup described below and shown schematically in Fig. 10 is ideally suited for detailed studies of the photon radiation and pair production processes in aligned crystals.

The radiator system comprised of the 178 GeV unpolarized electron beam focused on the single crystal silicon radiator (XTAL1). The crystal was of cylindrical shape with a 2.5 cm radius and a 1.5 cm thickness. It was aligned using a goniometer of 2 μrad precision to obtain either CB or SOS radiation conditions, as required. Upstream drift chambers (dch1up-2up) allowed tracking of the incoming beam with an angular precision of 4 μrad to define the position of incident electron in the incident angle phase space. The drift chambers had an active area of 15×15 cm^2 divided into six cells in both horizontal and vertical planes. A double sense wire configuration removed the directional hit ambiguity. The exit angles of the electron emerging from the radiator crystal was recorded by two tracking chambers (dch2up and dwc3). This allowed the measurement of electron multiple scattering angle inside the crystal. The dwc3 is a multi wire proportional chamber [52] with an active area of about 10×10 cm and a resolution of 200 μm.

The photon tagging system consisted of a dipole magnet (Bend8) capable of a maximum beam rigidity of 4.053 Tm and a special drift chamber (dch0) with no active horizontal cells. This constituted an upstream spec-

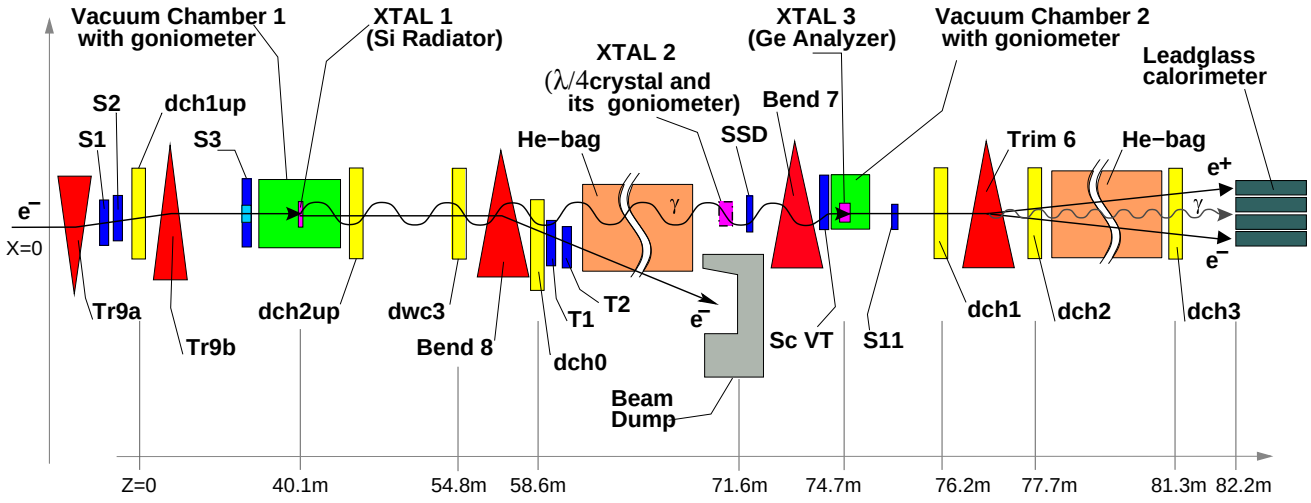

FIG. 10: The experimental setup.

trometer which measuredthe energy of the spent electron (with an acceptance of 10-90% of the incident energy). A beam dump protected the rest of the system from background effects arising from the spent electron.

The polarization analyzer system followed next. After passing a helium bag of length 9.65 m to reduce the multiple scattering, the remaining photon beam impinged on the analyzer crystal aligned with a goniometer of 20 μrad precision. The number of charged particles coming out of the analyzer crystal was counted both by a scintillator (S11) for fast triggering and a solid state detector (not shown) for offline analysis. The S11 scintillator was used to detect the photon conversion into e^+e^- pairs at the *analyzer* and it measured the number of charged particles seen right after the crystal *analyzer*. For the analysis, we only used events with 2MIPs in S11, as a signature for PP events. The photons which did not scatter or interact and the electron positron pairs created by the interacting photons continued into a magnetic spectrometer.

The pair spectrometer system was introduced next to measure the energy spectrum of the photon beam in a multi-photon environment. The dipole analysis magnet (Trim6) of the spectrometer was capable of a maximum beam rigidity of 0.53 Tm. The tracking elements upstream of the magnet consisted of one drift chamber (dch1) for the Ge analyzer and two drift chambers (dch05 and dch1) for the diamond analyzer. There were two drift chambers (dch2,dch3) downstream of the magnet. The drift chambers measured the horizontal and vertical positions of the passing charged particles with a precision of 100 μm yielding a spectrometer resolution of $\sigma_p/p^2 = 0.0012$ with p in units of GeV/c.

The calorimeter system measured E_γ^{tot}, the total radiated energy. This was done in a 12-segment array lead-glass calorimeter of 24.6 radiation lengths which had a resolution of $\sigma/E = 11.5\%/\sqrt{E}$, with E in units of GeV. The central segment of this lead-glass array was used to map and align the crystals with an electron beam [39].

A more detailed description of the NA59 experimental apparatus is reported elsewhere [53, 54].

Various plastic scintillators were used to calibrate the tracking chambers and to define different physics triggers. The normalisation event trigger (*norm*) consisted of the signal logic combination $S1{\cdot}S2{\cdot}\overline{S3}$ to ensure that an electron is incident on the radiator crystal. The scintillator Sc VT rejects radiation events coming from the conversion of the tagged photon beam upstream of the crystal *analyzer*. The radiation event trigger (*rad*) could then be defined as the signal logic combination $norm{\cdot}(T1.or.T2){\cdot}\overline{VT}$ indicating that the incoming electron has radiated and has been successfully taken out of the photon section of the beam line. The pair event trigger (*pair*) was constructed as the signal logic combination $rad{\cdot}S11$ to select the events for which at least one e^+e^- pair was created inside the analyzer crystal.

The three different experimental measurements described in this paper customised the experimental set-up as follows :

1. The measurement of the CPP cross section by linearly polarized photons on aligned crystals (birefringent effects in CPP) was performed using only the radiator and analyzer crystals. Both germanium and diamond analyzers were investigated. This measurement also established the new aligned crystal polarimetry technique.

2. The investigation of the conversion of linear polarization to circular polarization for the CB photons necessitated the inclusion of an additional crystal, denoted as the *quarter-wave plate*. The crystal polarimetry technique was extended to quantify circular polarization as well. The magnet B7 served as a sweeping magnet of the particles produced by electromagnetic showers in the *quarter wave plate*. A solid state detector SSD (500 μm thick Si crystal, $5{\times}5\,\mathrm{cm}^2$) was placed right after the *quarter wave*

FIG. 11: *Birefringent (quarter wave plate)* Si crystal and goniometer.

crystal during dedicated runs in order to study the shower development.

3. The measurement of the polarization of SOS radiation was done without the quarter-wave plate in the system, and in this case the radiator was configured to generate SOS radiation.

The case of the deployment of the quarter wave plate needs additional explanation. A third goniometer controlled the 10 cm thick Si <110> crystal, that served as a the quarter wave plate. It was located after the He-bag. A photograph of the quarter wave plate and the goniometer is shown in Fig. 11. The orientation of this crystal relative to the photon beam was already discussed in section III B (see Table I for a summary of the crystal parameters).

The axis of the Si crystal was carefully pre-aligned with respect to the axis of the azimuthal annular stage that was subsequently mounted into the main goniometer. This pre-alignment procedure was carried out at ESRF, Grenoble. A schematic of the alignment setup and the results are shown in Fig. 12. An X-ray reflection satisfying the Bragg condition was used to monitor the orientation of the the (110) crystallographic plane which is perpendicular to the <110> axis. The crystal was rolled in steps using the azimuthal goniometer stage (ϕ angle rotation). The <110> crystallographic axis was slightly misaligned with the crystal physical longitudinal axis and therefore also initially slightly misaligned with the azimuthal annular stage longitudinal axis. At each azimuthal step the Bragg condition had therefore to be recovered by adjustments to the angle of crystal face using a second goniometer (θ angle rotation). The Bragg condition was recognised by locating the two points at half-maximum of the Bragg peak. From a plot of the adjustment angle θ for each step in the roll angle ϕ of the azimuthal goniometer, the precise offset angles between the azimuthal goniometer longitudinal axis and the <110> crystallographic axis could be obtained. As the thick Si crystal was mounted in the azimuthal stage by adjustment screws, the <110> crystallographic axis could then be brought into coincidence with the longitudinal axis of the azimuthal goniometer.

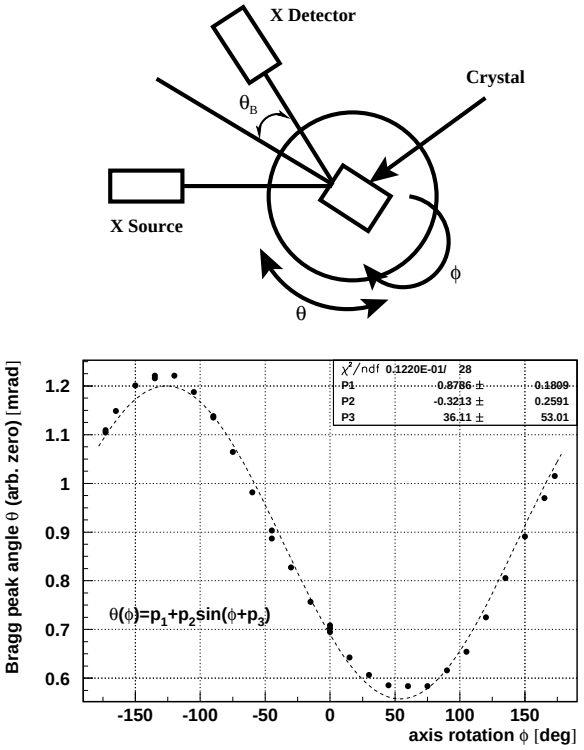

FIG. 12: Procedure and results for the annular stage alignment used to rotate the *quarter wave plate* crystal around the crystal axis.

The NA59 data acquisition system consisted of personal computers running the Linux operating system and using in-house developed software to access the VME and CAMAC readout crates containing the digitisation modules.The chamber signals were read out by VME TDC modules (Caen v767) with 1 ns resolution. The scintillator and calorimeter signals were read out with CAMAC ADC modules (LRS 2249) with 0.3 pC resolution. The raw data was then stored on DLT tapes for offline analysis.

TABLE I: Description of the angle settings for the quater wave plate set-up, where θ_0 is the angle between the photon momentum and crystal axis and ψ is the angle between the photon momentum and the indicated crystal plane.

Crystal Type	Purpose	Axes and Planes	Orientation	Thickness
Si	Radiator	<001>, (110)	θ_0=5 mrad, $\psi_{(110)}$=70 μrad	1.5 cm
Si	Quarter Wave Plate	<110>, (110)	θ_0=2.3 mrad, $\psi_{(110)}$=0	10 cm
Ge	Analyzer η_1 measurement η_3 measurement	<110>, (110)	θ_0=3 mrad, $\psi_{(110)}$=0 roll wrt radiator = $\pi/4$, $3\pi/4$ roll wrt radiator = 0, $\pi/2$	1 mm

B. Analysis

The first step in the offline analysis was the beam quality cuts, which ensured the consistency of various trigger ratios and the initial beam position and angles during data taking. Next, to facilitate comparison of the experimental results with theoretical predictions, the angular divergence of the electron beam was restricted to $\pm 3\sigma$ from its mean. Determination of the electron trajectory and its impact point on the radiator were essential for fiducial volume requirements. The radiated photons were taken to follow the direction of the initial electron. This is accurate to $1/\gamma \approx 5\mu$rad for 100 GeV electrons. To reconstruct the single photon energy in each event, only events where a single electron positron pair was manifest in the spectrometer volume with the pair energy being the same as the photon energy were selected. This subset of pair events were further classified into families according to the number of hits on the drift chambers of the spectrometer. In our nomenclature, "122 type" events are clearly the cleanest ones with one hit in the first upstream chamber, and two in both the second and third downstream drift chambers. The resulting pair production vertex was required to be in the fiducial volume of the analyzer crystal. For the case of the diamond analyzer, the additional drift chamber on the upstream side ensured a better vertex reconstruction. This in turn allowed us to veto the inter-tile events as well as the ones coming from the misaligned tile. Quality assessment of the pair search program was performed by a GEANT based Monte Carlo (MC) program. This program simulated the effects of the detector geometry to understand the precision and efficiency of the reconstruction algorithm for each event family.

TABLE II: Different material and angular settings for the analyzer crystal used to measure the linear polarization components.

analyser orientation (roll wrt radiator)	**analyzer type**	**measured polarization component**
$0, \frac{\pi}{2}, \pi, \frac{3\pi}{2}$	Ge	η_3
$\frac{\pi}{4}, \frac{3\pi}{4}, \frac{5\pi}{4}, \frac{7\pi}{4}$	Ge	η_1
$0, \frac{\pi}{2}$	Diamond	η_3

During the data taking, to obtain the parallel and perpendicular configurations, the angular settings of the radiator crystal (hence the direction of linear polarization of the photon beam) were kept constant. Only the analyzer crystal was rotated in a rolling motion around its symmetry axis. Therefore to measure the magnitude of the η_3 (η_1) component of the polarization, analyzer orientations separated by $\pi/2$ starting from 0 ($\pi/4$) were compared. To reduce the systematic errors, (especially in the case of the Ge crystal where the analysing power is smaller), all relevant angles on the analyzer crystal were utilised for polarization measurements, as presented in Table II. Other sources of systematic errors were the uncertainty in the crystal angles, the photon tagging and the pair reconstruction efficiencies obtained from MC studies.

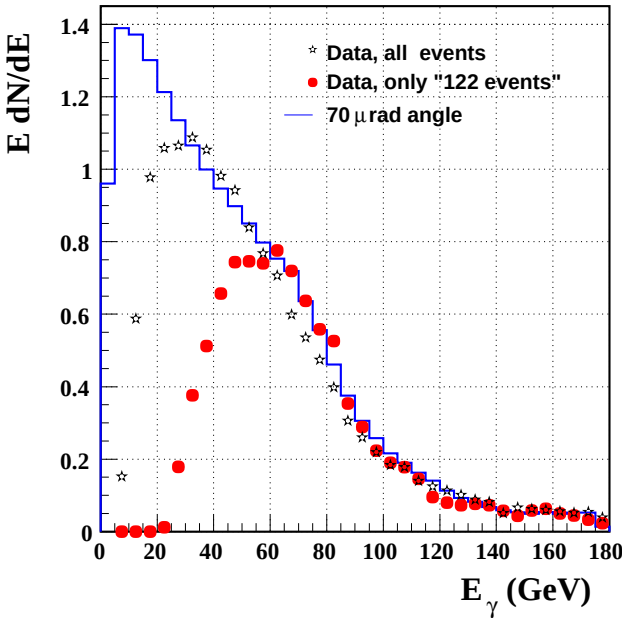

FIG. 13: MC predictions for the single photon spectrum, compared with data using all events (stars) and only '122 family' events (circles).

C. CB Validation

The angular settings of the radiator crystal was fine tuned by inferrence from the data. The single photon

intensity spectrum presented in Fig. 13 contains two different event selections superimposed on the MC prediction. The geometrical acceptance of the spectrometer for "122" events has a high threshold of 30 GeV, as seen from the Fig. 13.

An independent method of verifying the CB settings is looking at the total electromagnetic radiation from the radiator crystal. Fig. 14 shows the total energy radiated (EdN/dE) measured by the calorimeter for the radiator crystal aligned (bottom) and unaligned (top). In terms of the radiation intensity spectrum, an unaligned crystal is identical to an amorphous material. This radiation is called ICB and it can be approximated by the familiar Bethe-Heitler formula [55]. The increase in the CB radiation intensity spectrum is usually reported with respect to the IB spectrum. This ratio, called the "enhancement", is presented in Fig. 15 together with MC prediction for CB angle at 70 μrad. The agreement of the data with the enhancement prediction is remarkable. The offline analysis could therefore be used to monitor the angular settings of the radiator in time steps, to ensure the crystal angular settings did not drift during the measurement.

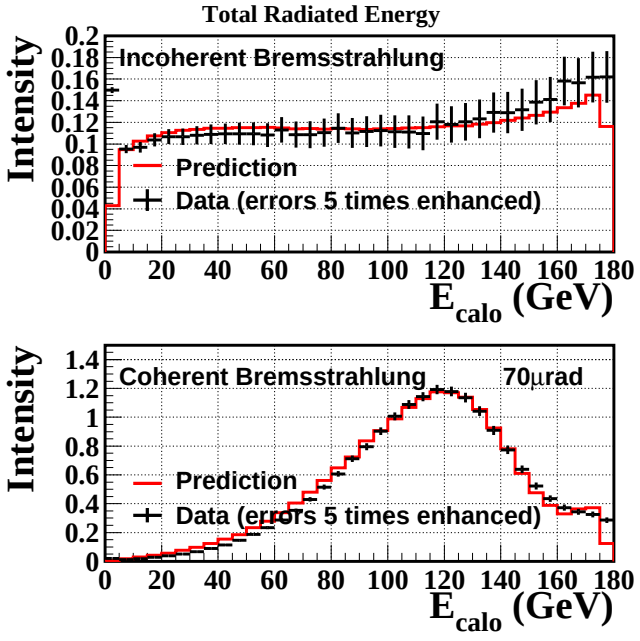

FIG. 14: Total energy radiated for Incoherent (top) and Coherent (bottom) bremsstrahlung radiation. The statistical errors on the data are enhanced by a factor of five to increase visibility.

V. RESULTS

A. Birefringence in CPP and a new crystal polarimetry

The orientation of the radiator crystal could be accurately determined by comparison of the predicted and measured CB enhancement (Fig. 15). The predicted and measured asymmetries for both linear polarization components: η_1 and η_3 could then be confidently compared. Using all events, as well as events passing the quasi-symmetrical pairs selection criteria, we see that, as expected, the asymmetry in Fig. 16 is consistent with zero yielding a vanishingly small η_1 component of the polarization.

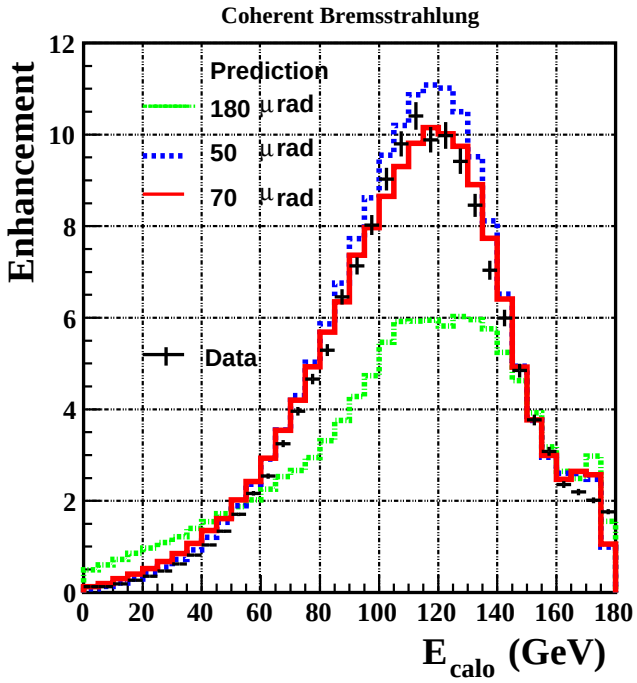

FIG. 15: Enhancement of CB radiation data compared to MC predictions. Note the sensitivity of the cross section to small changes in the angular setting of the crystal.

The measured asymmetry in the induced polarization direction (η_3) is presented in Fig. 17 without and with the y-cut using the Ge analyzer crystal. The solid line represents the MC predictions without any smearing in the spectrometer. The lower plot represents the increase in the asymmetry due to quasi-symmetrical pairs together with the statistical error associated with this increase. It thus confirms the non statistical source of the asymmetry increase in the 70-110 GeV range. The same polarization as measured by the diamond analyzer is given in Fig. 18. The top and middle plots show again the asymmetry measurements as compared to the MC predictions without any smearing, and the lower plot shows the increase in the asymmetry due to the y-cut. Comparing figures 17 and 18, we conclude that the multi-tile

synthetic diamond crystal is a better choice than the Ge crystal as an analyzer, since for the same photon polarization the former yields a larger asymmetry and thus enables a more precise measurement. The diamond analyzer also allowed the measurement of the photon polarization in the 30-70 GeV range, since it has some, albeit small, analyzing power at these energies.

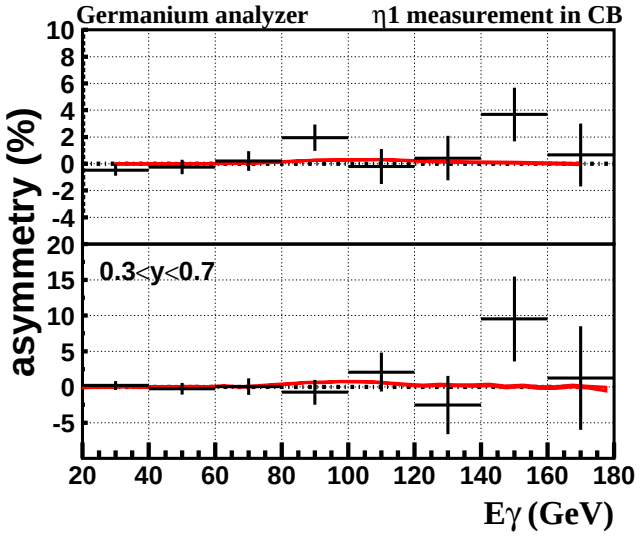

FIG. 16: Asymmetry to determined η_1 component of the photon polarization with the Ge analyzer. The data at roll angles $\pi/4+5\pi/4$ are compared to $3\pi/4+7\pi/4$ *without (TOP)* and *with (BOTTOM)* the quasi-symmetrical pair selection.

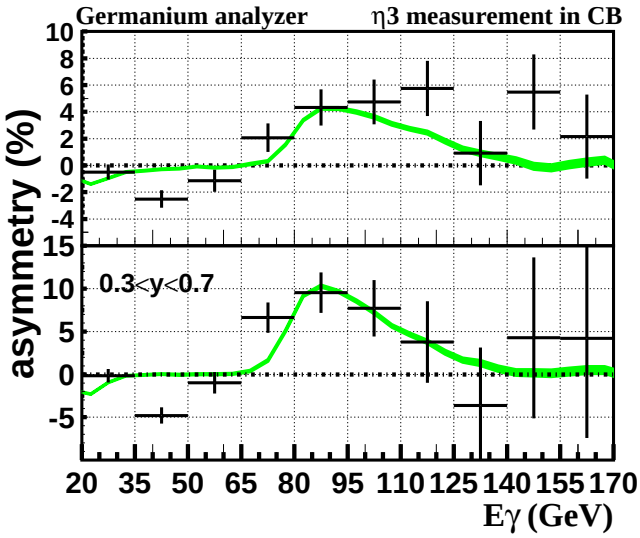

FIG. 17: Asymmetry to determine the η_3 component of the photon polarization with the Ge analyzer. Measurements *without (TOP)* and *with (BOTTOM)* the quasi-symmetrical pair selection at roll angles $0+\pi$ are compared to those at roll angles $\pi/2+3\pi/2$.

The theoretical predictions are based both on the calculation of the energy dependent polarization of photons

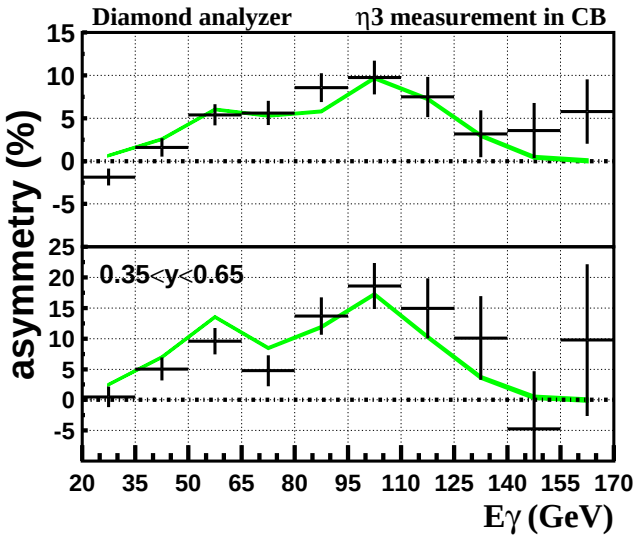

FIG. 18: Asymmetry measurements *without (TOP)* and *with (BOTTOM)* the quasi-symmetrical pair selection to determine η_3 component of the photon polarization with the *diamond* analyzer (Cf. Table II).

produced by coherent bremsstrahlung and the polarization dependence of coherent pair production, also as a function of incident energy. Thus the polarization sensitive versions of both CB and CPP are needed together in the theoretical calculation that predicts the measured asymmetry. The theoretical calculation combines the coherent and quasiclassical theories of radiation and pair production, in a Monte Carlo approach that can describe real beams with finite divergence. The agreement of this combined theory with the measured data is remarkable. It is clear that for the energy range of 30-170 GeV and the incident angle phase space of this study that the theory is sufficiently reliable and well understood to support the development of applications of crystals as polarimetry devices. The calculation of the resolving power (R in equation 6) is therefore reliable for the energy and angle regimes discussed in the introduction. The asymmetry measurements therefore correspond to a measurement of the induced polarization for CB for η_3 shown in Fig. 2. This has a maximum of 57% at 70GeV.

B. Conversion of linear to circular polarization

In this part of the experiment, the *quarter wave plate* crystal was introduced between the *radiator* and *analyzer* crystals. The linear polarization measurements mentioned in the previous section were extended to allow the measurement of circular polarization. This measurement is related to a reduction in linear polarization and the conservation of polarization. The theoretical background was described in section III B. It is noted that the expected and measured single photon spectrum for the chosen CB parameters for the *radiator* as shown in

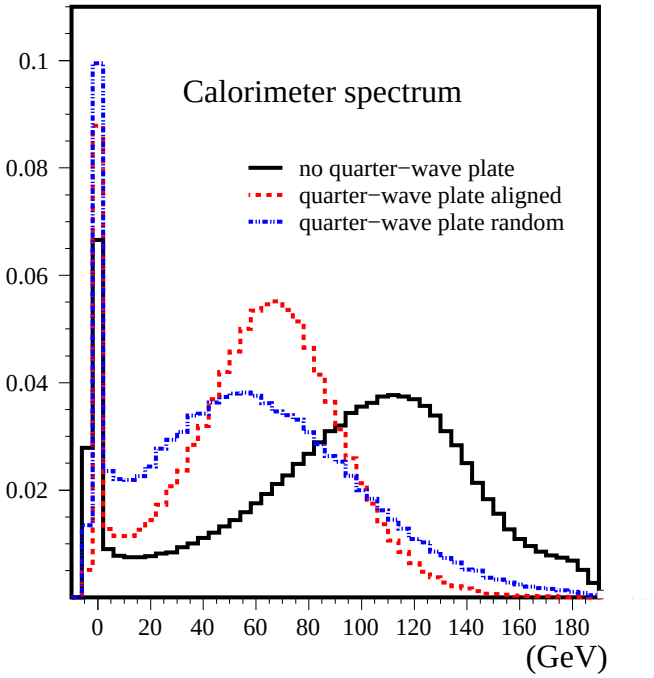

FIG. 19: Change in measured calorimeter energy spectrum for different settings of the *quarter wave crystal*. The shift in the peak energy is clear.

Fig. 13 are in good agreement. The expected polarization for the same set of parameters has already been given in Fig. 2 as a function of the single photon energy. As shown in the previous section, this polarization has been confirmed for the η_1 and η_3 components. This indicates that the linearly polarized CB photon beam is well understood.

Any change in the single photon spectrum after adding the *quarter wave crystal* will reflect how the incoming photons are absorbed or transformed by it. As η_1 was found to be consistent with zero before the *quarter wave crystal*, any nonzero value observed after it is a reflection of birefringent effects of the crystal.

Detailed theoretical calculations and simulations have been done to choose the crystal type, orientation and optimal thickness for the *quarter wave crystal*, leading to the choice of a 10 cm thick Si crystal as discussed above. The analysis took into account the real experimental parameters including the angular spread of the incident photon beam, the generation of secondary particles, multiple Coulomb scattering, and all particles produced by electromagnetic showers were also taken into account. In the simulation we assume the angular spread of the photons with energies between 70-100 GeV to be about $\sim$60 μrad and $\sim$45 μrad in horizontal and vertical planes, respectively, as measured from the data. The calculations also include the polarization transformation part for the surviving photon beam, resulting in elliptical polarization.

Fig. 19 shows the photon beam power spectrum measured with the LG electromagnetic calorimeter. The calorimeter sees all the surviving photons radiated by the parent electron. By comparing the spectrum with the *quarter wave crystal* at random and/or aligned with the case in which there is no *quarter wave crystal*, we can see that the *quarter wave plate* consumes a significant amount of the beam. This causes the peak energy of the pileup spectrum to be reduced by at least 50 GeV. However, it is also clear that the energy of the photons absorbed by the *quarter wave crystal* depends on its alignment condition.

As already mentioned, the prediction is that only 17-20% of the photons will survive in the energy region of interest. This is confirmed by the data, see Fig. 20. In addition, it is clear that the survival probability is also energy dependent as expected.

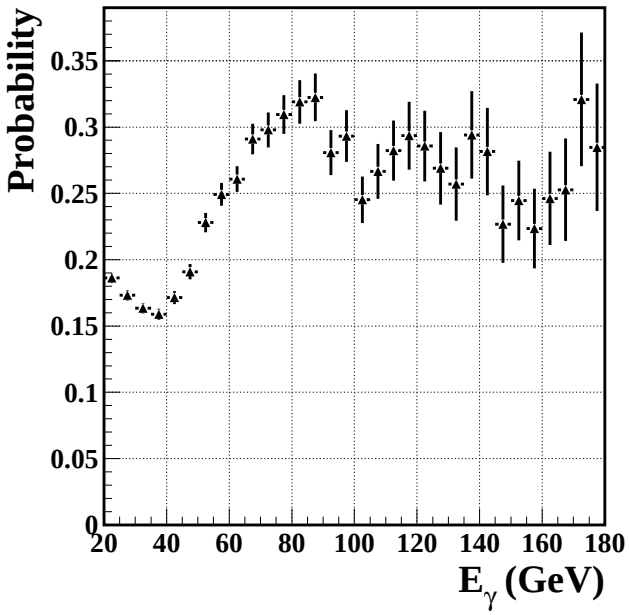

FIG. 20: Absorption probability found from the ratio of the single photon spectrum for the data with and without the *quarter wave crystal*.

Another consequence of adding the *quarter wave crystal* is a significant increase in the photon multiplicity of an event. For example, we expect an average multiplicity of three photons per electron for the nominal *radiator* settings. By analysing the correlation between the calorimeter spectrum and the single photon spectrum, we can conclude that the majority of these photons have energies <5 GeV, and that the calorimeter events at high energies are dominated by a single high energy photon and not due to the pileup of many low energy photons. As a consequence, the measurement of the Stokes parameters in the high energy range can be performed by measuring the asymmetry using either the calorimeter or the pair spectrometer.

The expected Stokes parameters and the total polar-

ization of the photons after the *quarter wave crystal* are given in Fig. 21. As shown, the expected value of the η_3 Stokes parameter decreases from 36% to 30% around 100 GeV. This difference should be seen in the PP asymmetry. The expected degree of circular polarization is of the order of ∼16% at the same energy. In Fig. 21, we expect an interesting increase of up to a factor of seven for the η_1 Stokes parameter in the same energy region. This phenomenon was also predicted by Cabibbo [56], the unpolarized photon beam traversing the aligned crystal becomes linearly polarized. This follows from the fact that the high-energy photons are mainly affected by the PP process. This cross section depends on the polarization direction of the photons with respect to the plane passing through the crystal axis and the photon momentum (polarization plane). Thus, the photon beam penetrating the oriented single crystal feels the anisotropy of the medium. For the experimental verification of this phenomenon with photon beams at energies of 9.5 GeV and 16 GeV, see [57, 58]. In the high energy region >100 GeV the difference between the PP cross sections parallel and perpendicular to the polarization plane is large. Since the photon beam can be regarded as a combination of two independent beams polarized parallel and perpendicular with respect to the reaction plane, one of the components will be absorbed to a greater degree than the other one, and the remaining beam becomes partially linearly polarized.

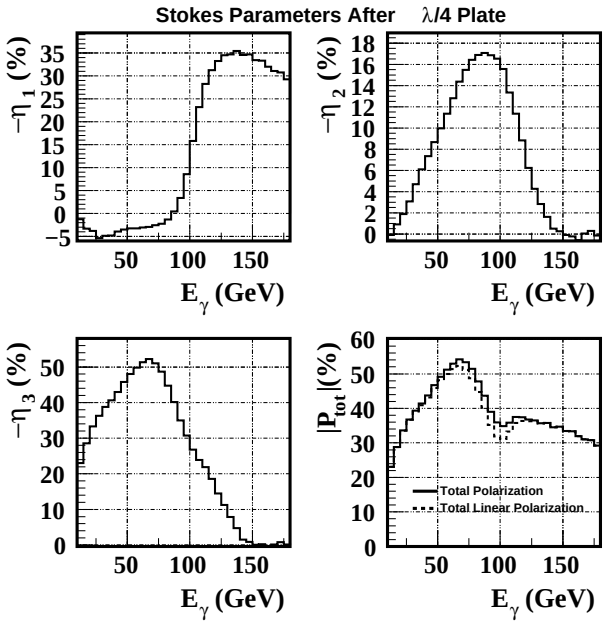

FIG. 21: Stokes parameters after the *quarter wave crystal*, assuming as input the values given in Fig. 2.

The data taking was limited to 18 hours due to a breakdown in the SPS that lead to a six day shutdown. As a consequence, we have a small data sample to test the predictions described above. The measured asymmetries using the calorimeter are given in Fig. 22 and again using the pair-spectrometer in Fig. 23. In order to reduce systematic uncertainties, the angular settings of the *radiator* crystal (hence the direction of linear polarization of photon beam) were kept constant, and only the *analyzer* crystal was rolled around its symmetry axis to obtain the parallel and perpendicular configurations. Therefore, to measure the polarization of the η_3 (η_1) component, the asymmetry between the 0 ($\pi/4$) and $\pi/2$ ($3\pi/4$) *analyzer* orientations were used.

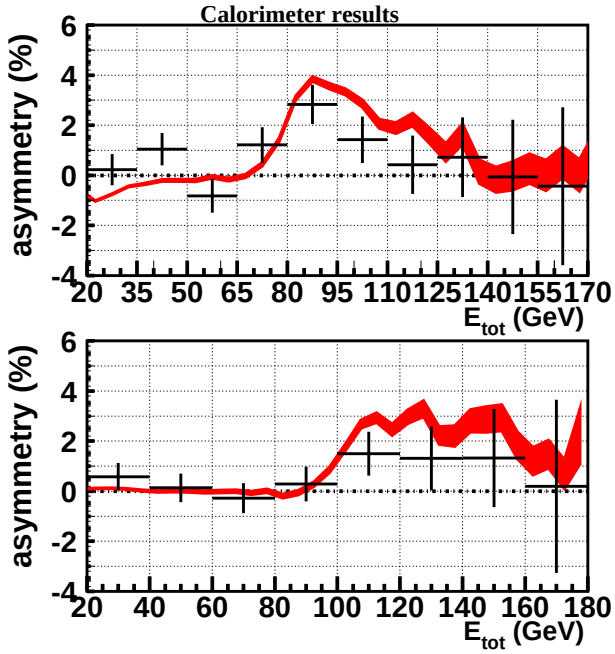

FIG. 22: Asymmetry measured with the calorimeter. The results reflects the changes in η_3 (top) and generation of η_1 (bottom) due to the presence of the *quarter wave crystal*.

As shown in these figures, the measured asymmetries are in agreement with the predicted polarization for the chosen Ge *analyzer* crystal setting [59]. For the Stokes parameter η_3, the measured asymmetry after the *quarter wave crystal* is about 2.9±0.7% in the energy range between 80-100 GeV. The estimated analysing power R for the Ge *analyzer* in the same energy range is about 10% [59]. Using the equation (6) one can estimate the measured Stokes parameter η_3 after the *quarter wave crystal*. Thus, the measured Stokes parameter is η_3=28±7% (see Fig. 21). For the Stokes parameter η_3, the measured asymmetry without the *quarter wave crystal* in the same energy range was found to be 4.7±1.7%, (see [59]). This corresponds to a measured value of η_3=44±11%, which is also consistent with the theoretically expected value of η_3, see Fig. 2.

Similar calculations may be done for the Stokes parameter η_1. If we make a weighted average for the asymmetry values between 20 and 100 GeV, where we expect no asymmetry, we obtain a value of 0.19±0.3%. Above 100 GeV we expect a small asymmetry, where we measured (1.4±0.7)% between 100 and 180 GeV.

Using the equation (14) one can now find the measured circular polarization degree which is equal η_2=21±11%. This is consistent with the predicted value of 16%.

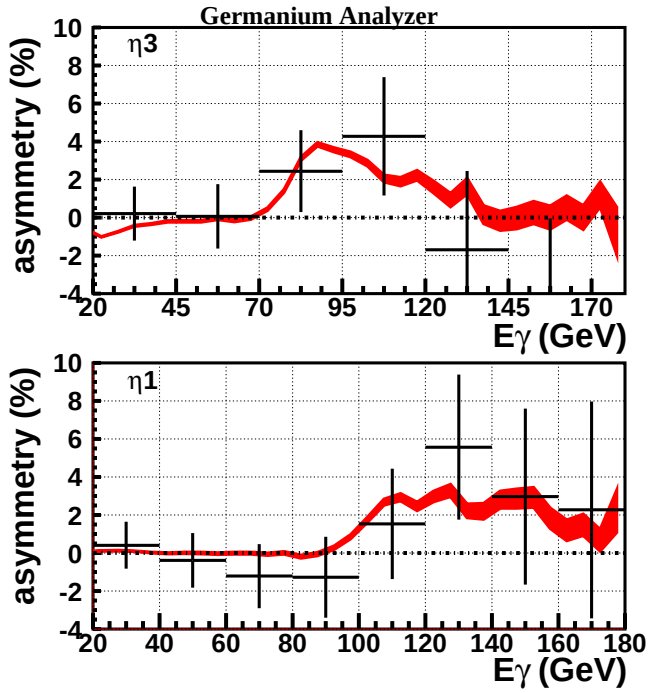

FIG. 23: Asymmetry measured with the pair spectrometer. The data sample with a fully reconstructed single e^+e^- pair is ten times smaller than the total data sample with at least one pair passing all the data quality cuts and with a 2MIPs cut in S11.

The statistical significance of the result was estimated using the F-test to evaluate the confidence level associated with distinguishing between two different statistical distributions. The first distribution was formed by the variance of the energy dependent data for the experimental circular polarization with respect to the theoretical prediction displayed in Fig. 21. The second distribution was formed by the variance of the same data to the null hypothesis prediction of no circular polarization. Limiting the test to the region where the crystal polarimeter has analysing power, and also to the region where the circular polarimetry technique of equation 14 has efficiency (80 - 110GeV), then we find a confidence limit of 73% for the observation of circular polarization.

C. Polarization measurement of SOS radiation

This third section of the experiment can be divided in two parts: (1) production of the photon beam by the photon radiation from the 178 GeV electron beam in the Si radiator oriented in the SOS mode and (2) measurement of the linear polarization using diamond crystals as analyzers. Prior to the experiment MC simulations were used to estimate the photon yield, the radiated energy, and the linear polarization of the photon beam and we optimized the orientation of the crystal radiator. The MC calculations also included the crystal analyzer to estimate the asymmetry of the e^+e^- pair production. The simulations further included the angular divergence of the electron beam, the spread of 1% in the beam energy, and the generation of the electromagnetic shower that develops in oriented crystals. To optimize the processing time of the MC simulation, energy cuts of 5 GeV for electrons and of 500 MeV for photons were applied.

1. *Photon Beam*

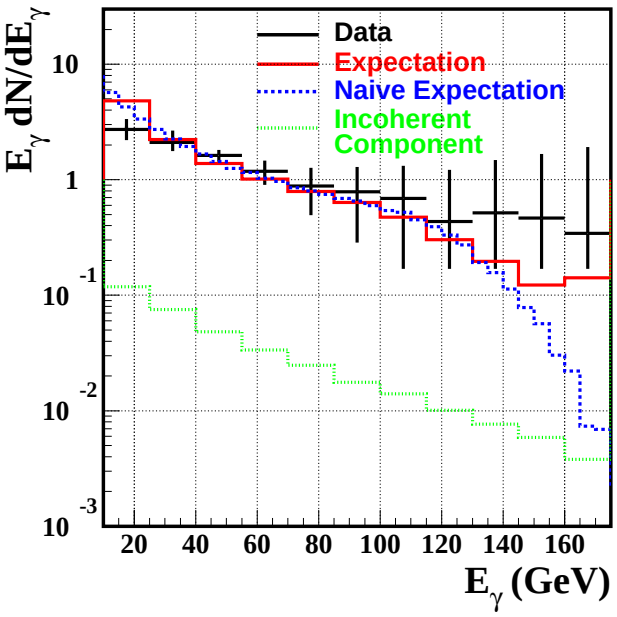

FIG. 24: Photon power yield, $E_\gamma dN/dE_\gamma$, as a function of the energy E_γ of individual photons radiated by an electron beam of 178 GeV in the SOS-aligned 1.5 cm Si crystal. The black crosses are the measurements with the pair spectrometer, the vertical lines represent the errors including the uncertainty in the acceptance of the spectrometer. The (red solid) histogram represent the MC prediction for our experimental conditions. The (green dotted) represent the small contribution due to incoherent interactions. For completeness, we also show the theoretical predictions if the experimental effects are ignored (blue dashed).

The SOS photons were produced as discussed in section II B and Fig. 3 displays a theoretical calculations of the various components of the photon power yield per unit of thickness of radiator crystal as used in the experiment. However there are several consequences for the photon spectrum due to the use of a 1.5 cm thick crystal. For the chosen orientation of the relatively thick Si crystal, the emission of mainly low energy photons from planar coherent bremsstrahlung results in a total average

photon multiplicity above 15. The most probable radiative energy loss of the 178 GeV electrons is expected to be 80%. The beam energy decreases significantly as the electrons traverse the crystal. The peak energy of both SOS and PC radiation also decreases with the decrease in electron energy. Consequently, the SOS radiation spectrum is not peaked at the energy for a thin radiator, but becomes a smooth energy distribution. Clearly, many electrons may pass through the crystal without emitting SOS radiation and still lose a large fraction of their energy due to PC and ICB. Hard photons emitted in the first part of the crystal that convert in the later part do not contribute anymore to the high energy part of the photon spectrum. A full MC calculation is necessary to propagate the predicted photon yield with a thin crystal, as shown in Fig. 3 for 178 GeV electrons, to the current case with a 1.5 cm thick crystal. This has been implemented for the measured photon spectrum shown in Fig. 24. We see that the measured SOS photon spectrum shows a smoothly decreasing distribution. Consequently, the high energy radiation is emitted essentially in the very first part of the crystal, while soft photons will be emitted along the full length of the crystal. This effect has been observed previously [15]. The low energy region of the photon spectrum is especially saturated, due to the abundant production of low energy photons. Above 25 GeV however, there is satisfactory agreement with the theoretical MC prediction, which includes the effects mentioned above.

The enhancement of the emission probability compared to the ICB prediction is given in Fig. 25 as a function of the total radiated energy as measured in the calorimeter. The maximal enhancement is about a factor of 18 at 150 GeV and corresponds well with the predicted maximum of about 20 at 148 GeV. This is a multi-photon spectrum measured with the photon calorimeter. The peak of radiated energy is situated at 150 GeV, which means that each electron lost about 80% of its initial energy due to the large thickness of the radiator. This means that the effective radiation length of the oriented single crystal is several times shorter in comparison with the amorphous target. The low energy region is depleted due to the pile-up of several photons.

The radiator angular settings were chosen to have the total linear polarization from the SOS radiation purely along η_3, that is $\eta_1 = 0$. The η_2 component is also zero because the electron beam is unpolarized. The expected η_3 (linear polarization) component of the polarization shown is in Fig. 26 as a function of photon energy. It is well known that channelling radiation in single crystals is linearly polarized [60, 61] and the low energy photons up to 70 GeV are also predicted to be linearly polarized in the MC simulations. High energy photons are predicted to have a small degree of polarization.

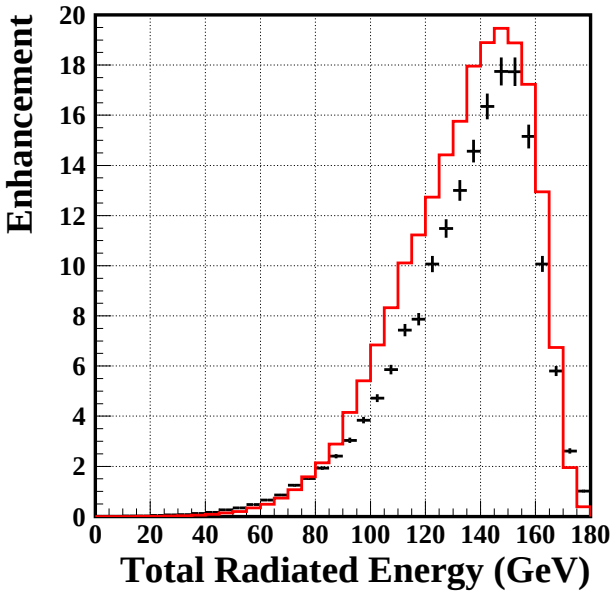

FIG. 25: Enhancement of the intensity with respect to the Bethe-Heitler (ICB) prediction for randomly oriented polycrystalline Si as a function of the total radiated energy E_{tot} in the SOS-aligned Si crystal by 178 GeV electrons. The black crosses are the measurements and the red histogram represent the MC prediction.

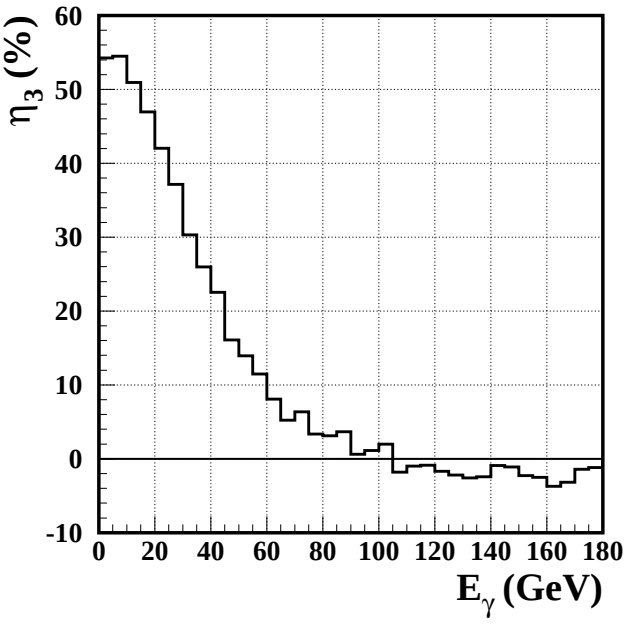

FIG. 26: Expected linear polarization as a function of the energy E_γ of the photons produced in the SOS-aligned Si crystal by 178 GeV electrons.

2. Asymmetry Measurement

The polarization measurement was made as explained in section III A. A multi-tile synthetic diamond crystal was used as an analyzer oriented with the photon beam at 6.2 mrad to the ⟨100⟩ axis and at 465 μrad from the (110) plane. This configuration is predicted to have a maximal analyzing power for a photon energy of 125 GeV as is shown in Fig. 27. The predicted analyzing power in the high energy peak region is about 30%.

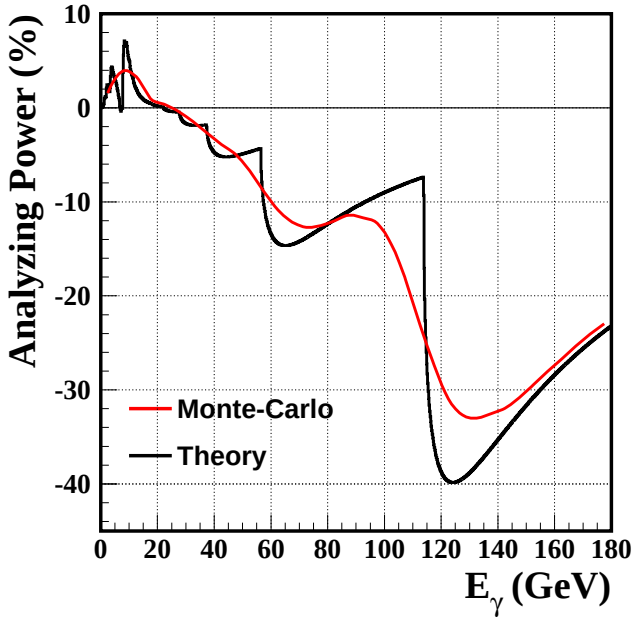

FIG. 27: Analyzing power R with the aligned diamond crystal as a function of the photon energy E_γ (black curve) for an ideal photon beam without angular divergence and (red curve) for the Monte Carlo simulation of photons with the beam conditions in the NA59 experiment.

The measured asymmetry and the predicted asymmetry are shown in Fig. 28. One can see that the measured asymmetry is consistent with zero over the whole photon energy range. For the photon energy range of 100-155 GeV we find less than 5% asymmetry at 90% confidence level using the F-test of significance. The null result is expected to be reliable as the correct operation of the polarimeter has been confirmed in the same beamtime in measurements of the polarization of CB radiation as described in secion V A. Note, that the expected asymmetry is small, especially in the high energy range of 120-140 GeV, where the analyzing power is large, see Fig. (27). This corresponds to the expected small linear polarization in the high energy range, see Fig. (26).

In contrast to the result of a previous experiment [32], our results are consistent with calculations that predict a polarization of only a few percent in the high energy photon peak for the SOS orientation. The analyzing power of the diamond analyzer crystal in the previous experiment's [32] setup peaked in the photon energy range of 20-40 GeV where a high degree of linear polarization is expected. But for that experiment in the high energy photon region we expect a small analyzing power of about 2-3%, also following recent calculation [34, 51]. The constant asymmetry measured in a previous experiment [32] over the whole range of total radiated energy may therefore not be due to the contribution of the high energy photons.

From Fig. 26 one can expect a large linear polarization for photons in the low energy range of 20-50 GeV. However, the analyzing power was optimized for an photon energy of 125 GeV and is small in the region where we expect a large polarization. A different choice of orientation of the analyzer crystal can move the analyzing power peak to the low energy range and may be used to measure the linear polarization in the low energy range.

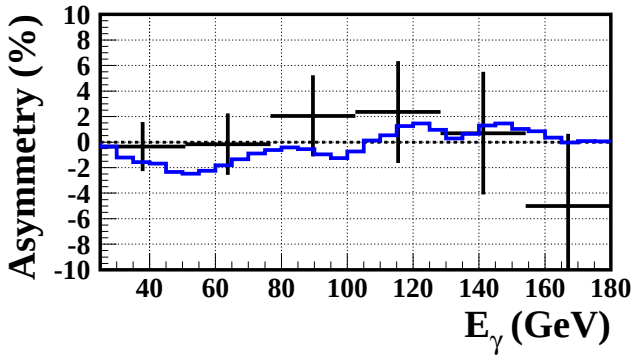

FIG. 28: Asymmetry of the e^+e^- pair production in the aligned diamond crystal as a function of the photon energy E_γ which is measured to determine the P_1 component of the photon polarization in the SOS-aligned Si crystal by 178 GeV electrons. The black crosses are the measurements and the red histogram represent the MC prediction.

VI. CONCLUSIONS

A. Birefringence in CPP and a new crystal polarimetry

Our results presented in this section show the feasibility of aligned crystals for linearly polarized high energy photon beams. From the experimental point of view, for the creation of a photon beam with a predictable spectrum the crucial components are (i) high precision goniometers to align the radiator crystal with respect to the electron beam and (ii) tracking chambers to monitor the incident angles of the electron beam on the crystal surface. The predictability of the photon energy and polarization is a good asset for designing future beamlines and experiments. The results also establish the applicability of aligned crystals as polarimeters for an accurate measurement of the photon polarization at high en-

ergies. The important aspects are the selection of the analyzer material and the utilization of quasi-symmetric pairs. The use of available synthetic diamond as analyzer crystal is found to be very promising due to its durability and high analyzing power.

The pair spectrometer enables us to do asymmetry measurements for single photons in a multi-photon environment. If the photon multiplicity is low, as it would be for laser generated beams with $E > 10\,\mathrm{GeV}$, then a simple multiplicity detector can be used to replace the more complex pair spectrometer. This is especially the case for a multiplicity detector which is energy selective. CB events with high photon multiplicity are known to be dominated by a single high energy photon and accompanied by multiple low energy photons.

The crystal polarimetry technique developed here will also be applicable in high energy photon beamlines as a fast monitoring tool. For example, in a future $\gamma\gamma$ or $e\gamma$ collider quasi-online monitoring of the photon beam polarization could be achieved using this crystal polarimetry method. In the most competitive designs of such colliders [62], the photon beam after the interaction region is transferred to a beam dump, hence the destructive nature of the crystal polarimetry technique does not constitute an impediment for its utilization.

B. Conversion of linear to circular polarization

The experimental results of this section show that coherence effects in single crystals can be used to transform linear polarization of high-energy photons into circular polarization and vice versa. Thus, it seems possible to produce circularly polarized photon beams with energies above 100GeV at secondary (unpolarized) electron beams at high energy proton accelerators. The birefringent effects becomes more pronounced at higher photon energy, which allows for thinner crystals with higher transmittance.

Diamond will be more efficient than silicon as quarter wave plates, and a 2 cm thick diamond crystal will have a transmission probability of about 80% for 100 GeV photons. A diamond array of 0.4 cm thickness was produced and aligned for our experiments, where we used it as a linear polarization analyzer, see Fig 6.

We did not perform an extensive measurement of the circular polarization from the decay asymmetry of ρ-mesons produced in and behind the birefringent Si crystal. This would have required additional beam time. However, with the aligned pair production crystal as an analyzer the realistic theoretical calculations describe very well (i) the radiated photon spectrum from the aligned radiator and (ii) the pair production asymmetries in the aligned analyzer with and without the birefringent Si crystal in the photon beam. In view of this good agreement all the predicted effects, including the birefringent effect, seem to be confirmed by the present measurements. Measurements of the charged particle multiplicity with depleted Si detectors show a large sensitivity to crystal alignments and can be used to control the alignment of crystals and the photon polarization in a future polarimeter set-up.

C. Polarization measurement of SOS radiation

We have performed an investigation of both enhancement and polarization of photons emitted in the so called SOS radiation mode. This is a special case of coherent bremsstrahlung for multi-hundred GeV electrons incident on oriented crystalline targets, where the hardness and the enhancement of the photon spectrum is more favourable than in the normal CB case. The experimental set-up had the capacity to deal with the relatively high photon multiplicity and single photon spectra were measured. This is very important in view of the fact that there are several production mechanisms for multiple photons which have different radiation characteristics. We have confirmed the single photon nature of the hard photon peak produced in SOS radiation.

The issue of the polarization of the SOS photons had previously not been settled conclusively. The results of an earlier experiment [32] indicated that a large polarization might be obtained for the high energy SOS photons. Our experimental results show that the high energy photons emitted by electrons passing through the Si crystal radiator oriented in the SOS mode have a linear polarization smaller than 20% at a confidence level of 90%.

Since the previous experiments, the theoretical situation for the polarization of hard SOS photons has also become clearer. Our results also confirm these recent calculations which predict that the linear polarization of high energy photons created in SOS orientation of the crystal is small compared to the polarization obtained with the PE orientation.

Photon emission by electrons traversing single crystals oriented in the SOS orientation has interesting peculiarities since three different radiation processes are involved: (1) incoherent bremsstrahlung, (2) channeling radiation and (3) coherent bremsstrahlung induced by the periodic structure of the atomic strings in the crystal that are crossed by the electron. The recent calculations have taken these three processes into account and predict around a 5% polarization for the high energy SOS photons. This prediction is consistent with our zero polarization result from the asymmetry measurement of single photons with energies above 100 GeV.

Acknowledgments

We dedicate this work to the memory of Friedel Sellschop. We express our gratitude to CNRS, Grenoble for the crystal alignment and Messers DeBeers Corporation for providing the high quality synthetic diamonds. We are grateful for the help and support of N. Doble, K.

Elsener and H. Wahl. It is a pleasure to thank the technical staff of the participating laboratories and universities for their efforts in the construction and operation of the experiment.

This research was partially supported by the Illinois Consortium for Accelerator Research, agreement number 228-1001. UIU acknowledges support from the Danish Natural Science research council.

[1] G. Baum et al., Compass Proposal, CERN/SPSLC 96-14, SPSLC/P297 (1996).
[2] Proposal on Spin Physics Using the RHIC Polarized Collider (RHIC-Spin Collaboration) (1992), update 1993.
[3] V. Ghazikhanian et al., SLAC Proposal E-159/160/161 (2000).
[4] A. Afanasev, C. E. Carlson, and C. Wahlquist, Phys. Rev. D **58**, 054007 (1998).
[5] H. Olsen and L. C. Maximon, Phys. Rev. **114**, 887 (1959).
[6] I. M. Nadzhafov, Bull. Acad. Sci. USSR, Phys. Ser. **14**, 2248 (1976).
[7] A. B. Apyan et al., Nucl. Instrum. Methods Phys. Res. B **145**, 142 (1998).
[8] R. Alley et al., Nucl. Instrum. Methods Phys. Res. A **365**, 1 (1995).
[9] J. L. Turner et al., Presented at EPAC'02, SLAC-PUB-9235 (2002).
[10] J. Lindhard, Kgl. Danske Videnskab. Selsk.: Mat.-Fys. Medd. **34**, 1 (1965).
[11] V. N. Baier, V. M. Katkov, and V. M. Strakhovenko, *Electromagnetic Processes at High Energies in Oriented Single Crystals* (World Scientific, Singapore, 1998).
[12] A. Apyan et al., hep-ex/0306028.
[13] A. Apyan et al., hep-ex/0306041.
[14] A. Apyan et al., hep-ex/0406026.
[15] K. Kirsebom et al., Nucl. Instrum. Methods Phys. Res. B **174**, 274 (2001).
[16] B. Ferretti, Nuovo Cimento **7**, 118 (1950).
[17] M. L. Ter-Mikaelian, *High Energy Electromagnetic Processes in Condensed Media* (Wiley Interscience, New-York, 1972).
[18] H. Uberall, Phys. Rev. **103**, 1055 (1956).
[19] G. Diambrini-Palazzi, Rev. Mod. Phys. **40**, 611 (1968).
[20] L. Criegee, G. Lutz, H. D. Schulz, U. Timm, and W. Zimmermann, Phys. Rev. Lett **16**, 1031 (1966).
[21] P. J. Bussey et al., Nucl. Instrum. Methods Phys. Res. **211**, 301 (1983).
[22] H. Bilokon et al., Nucl. Instrum. Methods Phys. Res. **204**, 299 (1983).
[23] R. Medenwaldt et al., Phys. Lett. B **281**, 153 (1992).
[24] J. Schwinger, Phys. Rev. **75**, 1912 (1949).
[25] J. Schwinger, Proc. Nat. Acad. Sci. **75**, 132 (1954).
[26] J. Schwinger, Phys. Rev. D **7**, 1696 (1973).
[27] A. Sorensen et al., Nucl. Instrum. Methods Phys. Res. B **119**, 1 (1996).
[28] Y. V. Kononets, Nucl. Instrum. Methods Phys. Res. B **33**, 22 (1988).
[29] K. Kirsebom et al., Phys. Rev. Lett. **87**, 054801 (2001).
[30] U. I. Uggerhoj, Rev. Mod. Phys. **77**, 1131 (2005).
[31] A. Saenz and H. Uberall, *Coherent Radiation Sources* (Springer-Verlag, Berlin, 1972).
[32] K. Kirsebom et al., Phys. Lett. B **459**, 347 (1999).
[33] V. N. Baier, V. M. Katkov, and V. M. Strakhovenko, Nucl. Instrum. Methods Phys. Res. B **69**, 258 (1992).
[34] S. M. Darbinian and N. L. Ter-Isaakian, Nucl. Instrum. Methods Phys. Res. B **187**, 302 (2002).
[35] V. M. Strakhovenko, hep-ph/0301149.
[36] V. M. Strakhovenko, Phys. Rev. A **68**, 042901 (2003).
[37] A. Apyan, (private communication).
[38] G. Barbiellini, G. Bologna, G. Diambrini, and G. Murtas, Nuovo Cimento **28**, 435 (1963).
[39] R. Moore et al., Nucl. Instrum. Methods Phys. Res. B **119**, 149 (1996).
[40] A. B. Apyan et al., Nucl. Instrum. Methods Phys. Res. B **173**, 149 (2001).
[41] K. Kirsebom et al., Nucl. Instrum. Methods Phys. Res. B **135**, 143 (1998).
[42] R. C. Burns et al., J. Cryst. Growth **104**, 257 (1990).
[43] J. P. F. Sellschop et al., New Diamond and Frontier Carbon Technology **10**, 253 (2000).
[44] J. Hoszowska et al., in *Proceedings of SPIE*, edited by A. K. Freund, T. Ishikawa, and A. M. Khounsary (2001), 4501, p. 106.
[45] A. Apyan et al., Proposal to the CERN SPS Committee, CERN/SPSC 98-17, SPSC/P308 (1998).
[46] N. Cabibbo et al., Phys. Rev. Lett. **9**, 270 (1962).
[47] G. D. Zorzi et al., in Polarization at LEP **2**, 64 (1988).
[48] Y. V. Kononets, (private communication).
[49] V. A. Maisheev, hep-ex/9904029.
[50] N. Z. Akopov, A. B. Apyan, and S. Darbinyan, hep-ex/0002041.
[51] V. M. Strakhovenko, Nucl. Instrum. Methods Phys. Res. B **173**, 37 (2001).
[52] J. Spanggaard, CERN SL-Note-98-023 (1998).
[53] R. Groess, Master's thesis, University of Witwatersrand, South Africa (2001).
[54] O. Wessley, Master's thesis, University of Witwatersrand, South Africa (2001).
[55] W. Heitler, *The Quantum Theory of Radiation* (Dover Publications, New-York, 1984).
[56] N. Cabibbo et al., Nuovo Cimento **27**, 979 (1963).
[57] C. Berger et al., Phys. Rev. Lett. **25**, 1366 (1970).
[58] R. L. Eisele et al., Nucl. Instrum. Methods Phys. Res. **113**, 489 (1973).
[59] A. Apyan et al., Nucl. Instrum. Methods Phys. Res. B **234**, 128 (2005).
[60] Y. N. Adishchev et al., JETP Lett. **33**, 462 (1981).
[61] S. A. Vorobyov et al., Sov. Phys. – JETP **94**, 38 (1988).
[62] NLC Zeroth Design Report, SLAC Report 474 (1996); Tesla Conceptual Design Report, DESY 1997-048 (1997).